www.czasopisma.pan.pl PAN www.journals.pan.pl
POLSKA AKADEMIA NAUK
Acta Geologica Polonica, Vol. 74 (2024), No. 4, e27
DOI: 10.24425/agp.2024.152659

Palaeoenvironmental indices (calpionellids, gamma-ray spectrometry, magnetic susceptibility) in the Berriasian of the Tisza Mega-unit (Lipse-tető section, Mecsek Mts, Hungary) and the Central Western Carpathians (lower Sub-Tatric succession, Tatra Mts, Poland) – a comparison

JACEK GRABOWSKI[1], DAMIAN GERARD LODOWSKI[1], ANDRZEJ PSZCZÓŁKOWSKI[2], LEONA CHADIMOVÁ[3], GEZA CSÁSZÁR[4†], KATARZYNA SOBIEŃ[1] and BALÁZS SZINGER[5]

[1] *Polish Geological Institute-National Research Institute, Rakowiecka 4, 00-975 Warsaw, Poland; e-mails: jacek.grabowski@pgi.gov.pl; damian.lodowski@pgi.gov.pl; katarzyna.sobien@pgi.gov.pl*
[2] *Institute of Geological Sciences, Polish Academy of Sciences, Warsaw Research Centre, Twarda 51/55, 00-818 Warsaw, Poland; e-mail: apszcz@interia.pl*
[3] *Institute of Geology of the Czech Academy of Sciences, v. v. i., Rozvojova 269, 165 00 Prague 6, Czech Republic; e-mail: chadimova@gli.cas.cz*
[4†] *deceased, Eötvös Loránd University, Pázmány Péter sétány 1/C, H-1117 Budapest, Hungary;*
[5] *EandP Laboratories, MOL Hungarian Oil and Gas Company,28 Dombóvári , H-1117 Budapest, Hungary; e-mail: szinger.balazs@gmail.com*

ABSTRACT:

Grabowski, J., Lodowski, D.G., Pszczółkowski, A., Chadimová, L., Császár, G., Sobień, K. and Szinger, B. 2024. Palaeoenvironmental indices (calpionellids, gamma-ray spectrometry, magnetic susceptibility) in the Berriasian of the Tisza Mega-unit (Lipse-tető section, Mecsek Mts, Hungary) and the Central Western Carpathians (lower Sub-Tatric succession, Tatra Mts, Poland) – a comparison. *Acta Geologica Polonica*, **74** (4), e27.

Calpionellid stratigraphy, magnetic susceptibility (MS) and gamma-ray spectrometry (GRS) have been investigated in the Berriasian pelagic limestones of ca. 21 m thick interval from the Lipse-tető section (Mecsek Mts, southern Hungary, Tisza Mega-unit). The section covers the lower and upper Berriasian (Calpionella and Calpionellopsis Zones respectively), however due to a thrust fault, the upper part of the Calpionella elliptica Subzone and the lower part of the Calpionellopsis simplex Subzone (lower/upper Berriasian boundary interval) were not documented. Reslults of GRS measurements reveal contrasting trends, with low detrital input (K, Th) and elevated Th/K ratio through the lower Berriasian, as well as relatively high detrital input and decreased Th/K ratio within the upper Berriasian. The differences occur also in the calpionellid frequencies and species richness: assemblages rich in *Calpionella alpina* dominate in the lower Berriasian, whilst more diversified yet less abundant associations characterize the upper Berriasian. Trends in palaeoenvironmental proxies correspond well with data from the Lower Sub-Tatric succession (Pośrednie-Rówienka composite section, Tatra Mts, Poland). The palaeoenvironmental change between the early and late Berriasian is most probably related to palaeoclimate (arid to humid transition), and fertility (from oligo- to mesotrophic regime). Trends documented in Th/K ratio might have been controlled by the intensity of aeolian transportation. As revealed by previous studies, the consistent record of palaeoenvironmental changes in both the Tisza Mega-unit and the Central Western Carpathians might be observed also in the middle Jurassic sediments.

Key words: Berriasian; Mecsek Mts; Tatra Mts; Biostratigraphy; Magnetic susceptibility; Gamma-ray spectrometry.

INTRODUCTION

The palaeoecology and palaeoenvironmental significance of Jurassic stromatolites played an important role amongst the scientific interests of Professor Michał Szulczewski (Szulczewski 1963, 1968). Although his investigations were essentially focused on the Polish sections (in the High-Tatric succession and the Polish Jura Chain), Professor M. Szulczewski described also stromatolitic structures from the Villány Mts in southern Hungary (Radwański and Szulczewski 1966). The authors noted the great similarity of the stratigraphic and sedimentary sequence in the Villány Mts, compared with that in the folded part of the High-Tatric succession, with transgressive Middle Jurassic lying directly above the Middle Triassic carbonate succession (Radwański and Szulczewski 1966). In both areas stromatolites are situated in the lowermost part of the transgressive succession (Łuczyński 2002; Vörös 2011), although their age estimations differ, pointing to Bathonian for the High-Tatric succession and Callovian for the Villány Hills. Despite their present-day separation and the fact that during the Mesozoic both areas likely belonged to different microplates (Central Western Carpathian and Tisza Mega-unit, respectively; see Text-fig. 1; Haas and Péró 2004; Szederkényi *et al.* 2012; Csaszar *et al.* 2013; Plašienka 2018), their common palaeotectonic history (i.e. the Middle Jurassic separation from the southern margin of the European plate, Late Jurassic–Early Cretaceous extension, and nappe stacking during the Late Cretaceous) along with their palaeogeographic proximity are widely accepted (e.g., Schmid *et al.* 2008). Accordingly, the Mesozoic succession of the Tisza Mega-unit was likely affected by a similar set of tectonic and palaeoenvironmental events as happened in other sedimentary zones located on the southern shelf of the Alpine Atlantic (e.g., Haas *et al.* 2011).

Recent studies in the Central West Carpathians and especially in the Lower Sub-Tatric succession (Grabowski *et al.* 2013; Jach *et al.* 2014; Grabowski and Sobień 2015; Jach and Reháková 2019) enabled dating and global correlations of some of sedimentary events in the Jurassic and Lower Cretaceous: the onset and demise of radiolarites (late Bathonian to early late Kimmeridgian), the development of nodular limestones (late Kimmeridgian–early Tithonian), or the widespread occurrence of calpionellid limestones around the Tithonian–Berriasian boundary and the onset of marly sedimentation during the late Berriasian. The main aim of this paper is to compare the sedimentary record of the pelagic Berriasian between the Tisza Mega-unit (Mecsek Mts) and the Lower Sub-Tatric succession of the Tatra Mts, and to discuss whether the similarity of successions, reported for the Middle Jurassic (Radwański and Szulczewski 1966) persists also in the lowermost Cretaceous deposits. The new data comprise biostratigraphy, magnetic susceptibility, stable isotope stratigraphy and gamma ray spectrometry (GRS) from the Lipse-tető section (Mecsek Mts), as well as hitherto unpublished GRS data from the composite Pośrednie-Rówienka section (Western Tatra Mts).

GEOLOGICAL SETTING

The Mecsek Mts is a relatively small mountain range located in southern Hungary, just north of the city of Pécs (Text-fig. 1). Together with a nearby Villány Hills they form the only tectonic window in the area of Hungary which provide an insight into the pre-Neogene basement of the Tisza (Tisia) Mega-unit (Text-fig. 1B). Right after the Variscan accretion the Tisza Mega-unit occupied a position on the southern margin of the European Plate, constituting part of the northern Tethyan (Neotethyan) shelf (Haas and Péró 2004; Szederkényi *et al.* 2012; Haas *et al.* 2014). The opening of the Alpine Atlantic (Ligurian–Penninic or Alpine Tethys) oceanic branch during the Middle–Late Jurassic (Text-fig. 1D) led to separation of the Tisza microplate from the stable continent. This process resulted also in the formation of the two basinal zones separated by a horst in between (Villány–Bihor Zone): the Mecsek Basin (Zone) to the north, and the Békés–Codru Basin (Zone) to the south (Text-fig. 1E).

After the Tisza Mega-unit separated from the European Plate, pelagic sedimentation prevailed in the Mecsek Zone: occasional radiolarites and more typical siliceous marls and limestones (Dorogó Marl and Fonyászó Limestone formations; Callovian–Oxfordian), *Ammonitico Rosso*-type red nodular limestones (Kisújbánya Limestone, Kimmeridgian–lower Tithonian), as well as *Maiolica*-type limestones with cherts (Márévár Limestone; Upper Tithonian–Berriasian). Characteristic of the upper part of the Márévár Fm is the occurrence of volcanic bombs, which announced a period of intense basalt magmatism during the Valanginian–Hauterivian. The Early Cretaceous volcanism brought also the formation of atoll-like carbonate build-ups; the areas where the magmatism was less intense were occupied by crinoidal meadows (e.g., Császár 2002; Szinger 2008; Szederkényi *et al.* 2012; Haas *et al.* 2014).

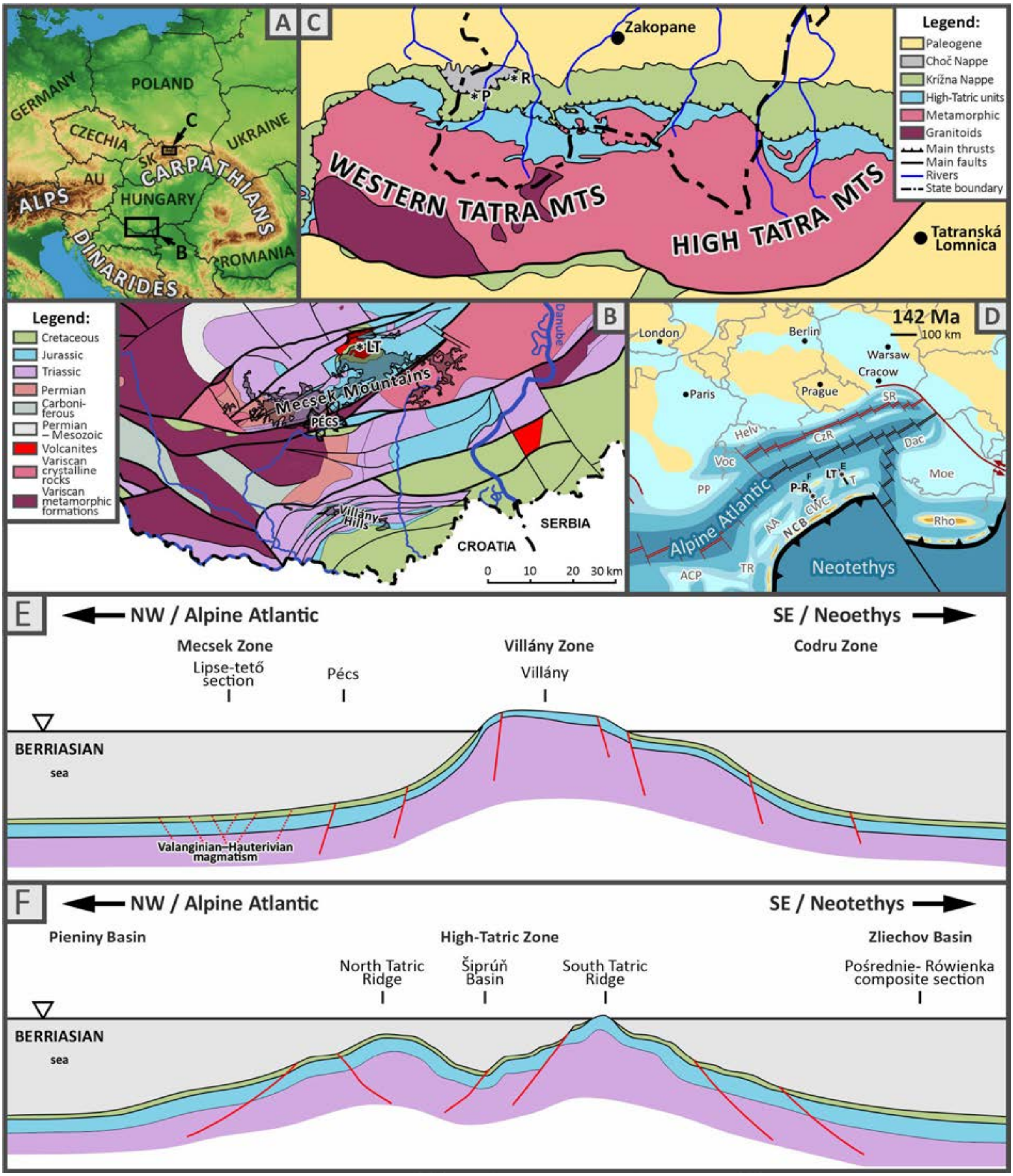

Text-fig. 1. Geological context of the studied area. (A) Geographical location of the Mecsek and Tatra Mts. (B) Pre-Cenozoic geological map of the Mecsek Mts and the neighbouring area with location of the Lipse-tető section (simplified after Haas *et al*. 2011). (C) Simplified tectonic sketch-map of the Tatra Mts (modified after Nemčok *et al*. 1994 and Jurewicz 2005) with location of Pośrednie II–III (P) and Rówienka sections (R). (D) Simplified paleogeographical map of the circum Carpathian region during the early Berriasian (modified after Stampfli and Hochard 2009; Lodowski *et al*. 2024). (E–F) Conceptual cross section of the latest Jurassic–earliest Cretaceous structures of the Tisza Mega-unit (Mecsek, Villány and Codru zones) and Central Western Carpathians. Abbreviations: LT – Lipse-tető section; P-R – Pośrednie-Rówienka composite section; AA – Austro Alpine; ACP – Adriatic Carbonate Platform; CWC – Central Western Carpathians; Dac – Dacia; NCB – Neotethyan Collision Belt; CzR – Czorsztyn Ridge; Helv – Helvetic units; Moe – Moesian Platform; PP – Provencal Platform; Rho – Rhodopes; SR – Silesian Ridge; TR – Transdanubian Range; Voc – Vocontian Basin.

In the Mecsek Mts, Cretaceous formations younger than Barremian were most likely eroded during the late Albian–Cenomanian, when the first phase of Alpine orogeny affected the area; in addition intense nappe stacking during the Coniacian has been documented from the eastern part of the Tisza Mega-unit in the Apuseni Mts, Romania (Szederkényi *et al.* 2012).

The Jurassic–Cretaceous sedimentary sequence of the Lower Sub-Tatric succession (Central Western Carpathians) provides a record of the birth and closure of the extensional Zliechov Basin. Back in the Late Jurassic–Early Cretaceous it was located in between the High-Tatric Ridge (to the north) and the Cimmerian wedge (Neotethyan Collision Belt) to the south (Text-fig. 1F). It consists of pelagic and hemipelagic sediments (Lefeld 1974; Vašiček *et al.* 1994; Michalík 2007), comprising variegated radiolarites of Oxfordian–late Kimmeridgian age (Sokolica and Czajakowa Radiolarite Formations), upper Kimmeridgian–lower Tithonian nodular and platy limestones of the Czorsztyn and Jasenina Formations (Lefeld *et al.* 1985; Grabowski and Pszczółkowski 2006; Jach *et al.* 2014; Jach and Reháková 2019), Berriasian calpionellid limestones of the Osnica Fm (Grabowski and Pszczółkowski 2006; Grabowski *et al.* 2013) and upper Berriasian–Aptian marls and marly limestones of the Kościeliska Marl Formation (Lefeld *et al.* 1985; Pszczółkowski 2003). After the Cenomanian, the Zliechov Basin was closed and thrust northwards together with other tectonic elements of the Hronic nappe system (e.g., Plašienka, 2018), forming the present-day Lower Sub-Tatric (or Križna) nappe (Text-fig. 1C).

Sections description

Lipse-tető

The Lipse-tető section is located in an abandoned quarry, in the eastern part of the Mecsek Mts, on the foothills of Lipse-tető hill, directly south of the village Szászvár (Text-fig. 1). Earlier studies focused on another section (comparable to the subject of this study) on the opposite side of the quarry which provided a more complete Berriasian record. Based on calpionellid investigations (Szinger and Császár 2010; Nagy and Szinger 2012) the limestone was formed during the early and late Berriasian. This study provides the first comprehensive stratigraphic and palaeoenvironmental study of the new section. It utilizes the data collected in ca. 21 m thick interval spanning the lowermost to upper Berriasian of the Márévár Formation (Text-fig. 2; see also Pl. 1).

The basal part of the section (ca. 0–4 m) is made of gray, thin- and medium-bedded limestone. The interval between 2.5–3.5 m shows some traces of dissolution, possibly late stylolite-type. The bedding becomes thicker above, exceeding 0.5 m and reaching up to 1 m (bed 21, ca. 6 m). At the 9.6 m horizon the succession is cut by a thrust fault. Above (beds 26–44) the bedding is thin and/or very thin again, whereas within the 14.5–15.6 m interval a slump is observed (bed 45). Thin bedded limestone continues above, up to the top of the interval studied at bed 57 (ca 20.5 m).

Pośrednie-Rówienka composite section

The Pośrednie II and III sections are located west of the Chochołowska Valley, on the ridge between the Kryta and Długa valleys (Pszczółkowski 1996; Grabowski and Pszczółkowski 2006). The Rówienka section is situated in the lower part of the Lejowa Valley, in a gully on its south-east slopes (Grabowski and Pszczółkowski 2006) (Text-fig. 1C). Despite some observational gaps, the three sections cover the complete upper Tithonian–upper Berriasian interval, between magnetozones M20r and M16n, from the Chitinoidella Zone to the Calpionellopsis oblonga Subzone (Grabowski and Pszczółkowski 2006). Accordingly, the three sections are compiled here into a synthetic, ca. 80 m thick composite section. It consists of three distinct lithostratigraphical units: platy limestones of the Jasenina Formation (upper Tithonian and the lowermost Berriasian), pale micritic limestones of the Osnica Formation (lower Berriasian) and marly limestones and marls of the Kościeliska Marl Formation (upper Berriasian). The boundaries between the formations are situated in the lowermost Calpionella alpina Subzone (Jasenina Fm/Osnica Fm) and at the transition between the Calpionellopsis simplex and Cps. oblonga Subzones (Osnica Fm/Kościeliska Marl Fm) (Grabowski and Pszczółkowski 2006; Grabowski and Sobień 2015).

Each of the three formations mentioned above bears specific rock magnetic and geochemical characteristics, which are likely related not only to regional but also supra-regional paleoenvironmental trends (Grabowski and Pszczółkowski 2006; Grabowski *et al.* 2013). GRS and chemostratigraphic data (main and trace elements) from the Pośrednie III section were previously published by Grabowski *et al.* (2013); this paper supplements the archive data with hitherto unpublished GRS results from the Pośrednie II and Rówienka sections (28 and 35 m of thickness, respectively).

MATERIALS AND METHODS

All the numerical data supporting the findings of this study are available as Appendix 1.

Calpionellid biostratigraphy

A total number of 57 thin sections were prepared from the 21 m thick interval of the Lipse-tető section. Calpionellids were investigated using a Nikon ECLIPSE LV100POL polarizing microscope (Institute of Geological Sciences, Polish Academy of Sciences), adopting the calpionellid zonation of Lakova and Petrova (2013). The calpionellid biostratigraphy of the Pośrednie-Rówienka composite section was published in Grabowski and Pszczółkowski (2006).

Magnetic susceptibility and rock magnetism

Magnetic susceptibilities (MS) of 199 stratigraphic horizons of the Lipse-tető section (with mean resolution of ca. 10 cm) were measured during the field work using a ZH Instruments SM30 Magnetic Susceptibility Meter; MS of each horizon was measured three times in order to calculate its mean value. 74 horizons were intended for sampling and laboratory investigations of rock magnetic properties in the Paleomagnetic Laboratory of the Polish Geological Institute-National Research Institute (PGI-NRI). Rock samples were crushed into a homogenous fine-gravel fraction and packed in 8 cm^3 sample boxes. Laboratory investigations comprised mass-normalized measurements of the MS and natural remanent magnetization (NRM), as well as laboratory induced magnetizations: isothermal remanent magnetization (IRM) and anhysteretic remanent magnetization (ARM). MS measurements were performed using an Agico KLY2 kappabridge. IRM was applied along the Z axis in the field of 1 T (IRM_{1T}) and then antiparallel in the field of 100 mT (IRM_{100mT}) using a Magnetic Measurements MMPM Pulse Magnetizer. ARM was produced in a Molspin device with peak alternating field of 100 mT and a steady field bias of 0.1 mT. NRM, IRM and ARM measurements were processed using an Agico JR6A spinner magnetometer and Agico Rema6 software. S-ratio ($-IRM_{100mT}/IRM_{1T}$) was calculated in order to indicate the proportions between low and high coercivity minerals (i.e. Opdyke and Channell 1996). The low coercivity fraction (i.e. magnetite) is characterized by high S-ratio values (above 0.6), whilst the lower S-ratio accounts for the admixture of high coercivity minerals, e.g. hematite or goethite.

Gamma-ray spectrometry

Field gamma-ray spectrometric measurements in the Lipse-tető and Pośrednie-Rówienka sections were carried out using a Radiation Solution RS-232 portable natural radioisotope assay analyzer with BGO 2×2” detector. Energy windows of potassium, uranium and thorium were analyzed in 300 s time intervals. The results account for the value of the total dose (nGy/h), SGR (standard gamma-ray; ppm), counts per minute (cpm) for K, U and Th as well as their converted concentrations (% for K and ppm for U and Th). A total number of 98 measurements was performed in the Lipse-tető section every 10–30 cm, with mean resolution 20 cm. New GRS data from the Lower Sub-Tatric succession embrace the Pośrednie II and Rówienka sections (35 and 68 measurements, respectively; mean resolution 0.5 to 1 m). Those were integrated with already published GRS data from the Pośrednie III section (Grabowski *et al.* 2013). In order to estimate the total amount of terrigenous influx the CGR (computed gamma-ray) index was calculated following the formula: CGR [API] = Th [ppm] × 3.93 + K [%] × 16.32 (Rider 1999; Kumpan *et al.* 2014).

The set of collected data allow also some basic interpretation of the paleoenvironmental conditions during sedimentation. In order to estimate whether the sediments were subjected to oxygen depletion, the U/Th ratio was calculated. The Th/K ratio is often used as a paleoclimate indicator (i.e. Ruffel and Worden 2000; Schnyder *et al.* 2006), where lowered K content (relative to Th) results from warm and humid hinterland paleoclimate and the associated process of K-leaching from clays.

Stable carbon and oxygen isotopes

A total number of 55 bulk rock samples were prepared for $\delta^{13}C$ and $\delta^{18}O$ analysis in the Lipse-tető section. Analyses were carried out in the Stable Isotope Laboratory of the GeoZentrum Nordbayern, Erlangen, Germany. Carbonate powders were analyzed using a Gasbench II connected to a ThermoFisher Delta V Plus mass spectrometer. All values are reported in per mil relative to V-PDB scale. Oxygen and carbon isotope values are reported in per mil relative to VPDB scale by calibration to the accepted values of NBS 19 ($\delta^{13}C$ = +1.95‰; $\delta^{18}O$ = -2.20‰) and LSVEC ($\delta^{13}C$ = -46.6‰; $\delta^{18}O$ = -26.7‰) references. Reproducibility of measurements was monitored by replicate analysis of laboratory standards Erl 5 (n = 12) and Sol 2 (n = 17). Reproducibility for both $\delta^{13}C$ and $\delta^{18}O$ was 0.06‰

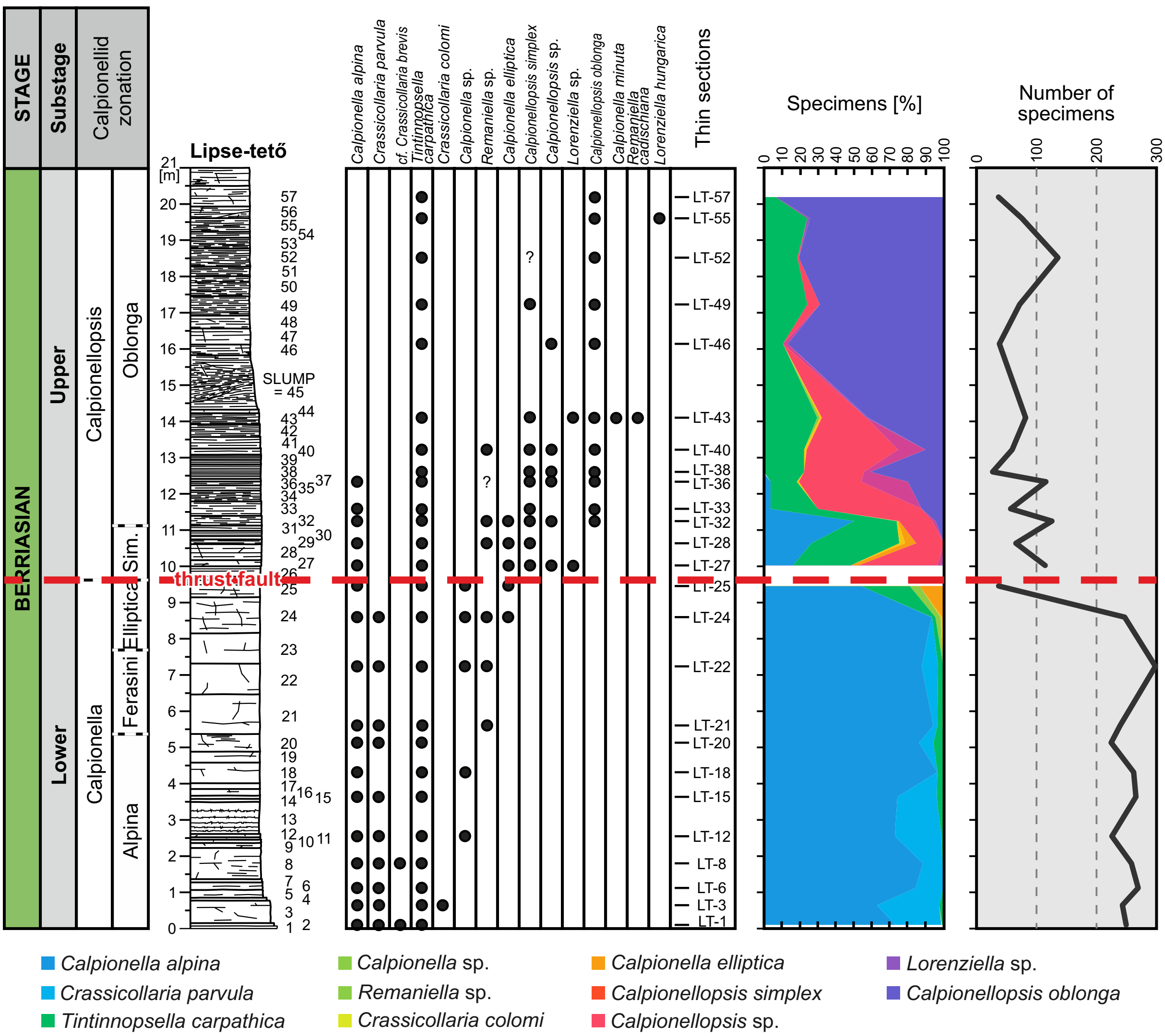

Text-fig. 2. Calpionellid stratigraphy, taxa ranges, percentage share and the total number of calpionellids in the Lipse-tető section. Abbreviations: Sim. – Simplex.

and 0.04‰ (± 1σ) for Erl 5 as well as 0.04‰ and 0.05‰ (± 1σ) for Sol 2.

RESULTS

Microfacies of the Lipse-tető section

Wackstones which are a light grey and grey, generally thin- to medium-bedded, laminated, homogenous biomicrite prevail, throughout the section. The microfauna is dominated by the calpionellids. The microfossil assemblage – beside calpionellids – is represented by radiolarians, calcareous dinocysts and globochaetes. The determinated calcareous dinocysts are *Pithonella* sp., *Cadosina fusca*, ?*Cadosina semiradiata*, and *Colomisphaera* sp. Most of the radiolarians are recrystallised. Other benthic biogenic constituents are present in subordinate amounts. They comprise mollusc shell fragments, sparse benthic foraminifera (*Spirillina* sp., *Nodosaria* sp., *Textularia* sp.), and echinoderm fragments. sp. Upwards in the section, the amount of calpionellids decreases, while the radiolarians become dominant.

Calpionellid biostratigraphy and frequencies in the Lipse-tető section

The Calpionella alpina Subzone is about 5.4 m thick and contains a typical early Berriasian calpionel-

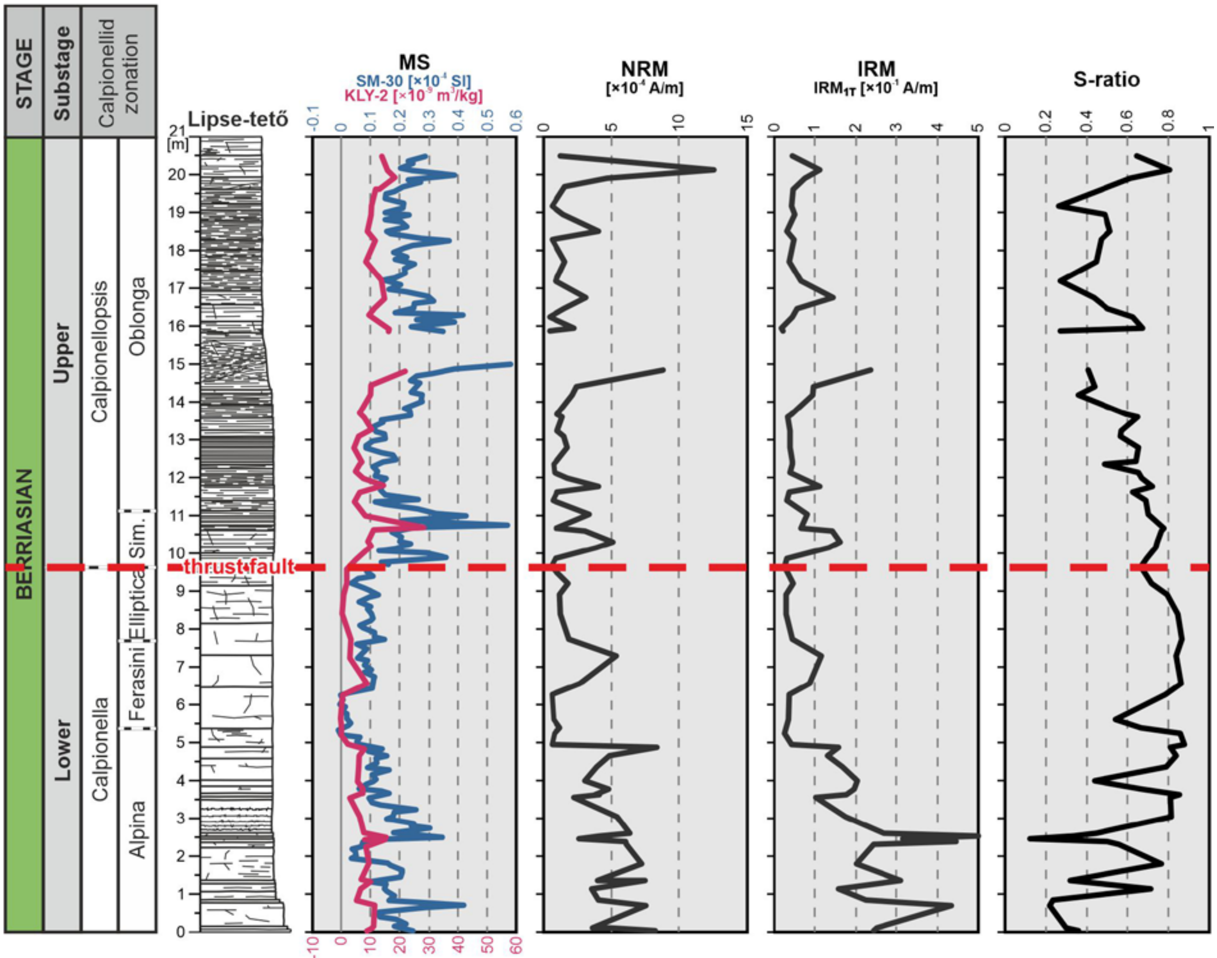

Text-fig. 3. Field (SM-30) and laboratory measured (KLY-2) magnetic susceptibility (MS), natural remanent magnetization (NRM) isothermal remanent magnetization acquired in the field of 1 T (IRM_{1T}), and S-ratio within the Berriasian of the Lipse-tető section. NRM and IRM_{1T} values are normalized to 10 g. Abbreviations as on Text-fig. 2.

lid assemblage with *C. alpina*, *Crassicollaria parvula*, *Tintinnopsella carpathica* and a few specimens identified as *Calpionella* sp. Even though a single specimen of *Crassicollaria colomi* was found in sample LT-3 this cannot be treated as an argument for its late Tithonian age (Crassicollaria colomi Subzone *sensu* Pop, 1994; Reháková and Michalík, 1997; Michalík *et al.* 2009), since the taxon is known to occur within the lower Berriasian beds, sometimes even as high as in the upper part of the Alpina Subzone (Lakova and Petrova 2013; Petrova *et al.* 2019, 2023). The boundary with the Remaniella ferasini Subzone (Text-fig. 2) is marked by the occurrence of *Remaniella* sp., yet the index taxon (*R. ferasini*) was not identified; the subzone is only about 2 m thick. Next, the Calpionella elliptica Subzone is about 2 m thick, however, its upper boundary is tectonic (thrust fault; Text-fig. 2; see also Pl. 2).

The limestone above the thrust fault belongs to the late Berriasian Calpionellopsis simplex Subzone (1.4 m in thickness). The radiolarian microfacies is typical for this part of the section. The following Calpionellopsis oblonga Subzone is about 10 m thick; it is characterized by thin bedded radiolarian limestones with *Calpionellopsis oblonga* (mainly), but also *Tintinnopsella carpathica*, *Calpionellopsis simplex* and some other, less frequent taxa (Text-fig. 2). The specimens of *Calpionellopsis simplex* do occur up to sample LT-49, but are not seen higher in the section. The topmost part of the section (samples LT-55 and 57) yielded *Calpionellopsis oblonga*, *Tintinnopsella carpathica* and *Lorenziella hungarica*, only. This interval probably corresponds to zone "no. 17" proposed by Nagy (1986, tab. II). Radiolarian microfacies predominates the entire Oblonga Subzone,

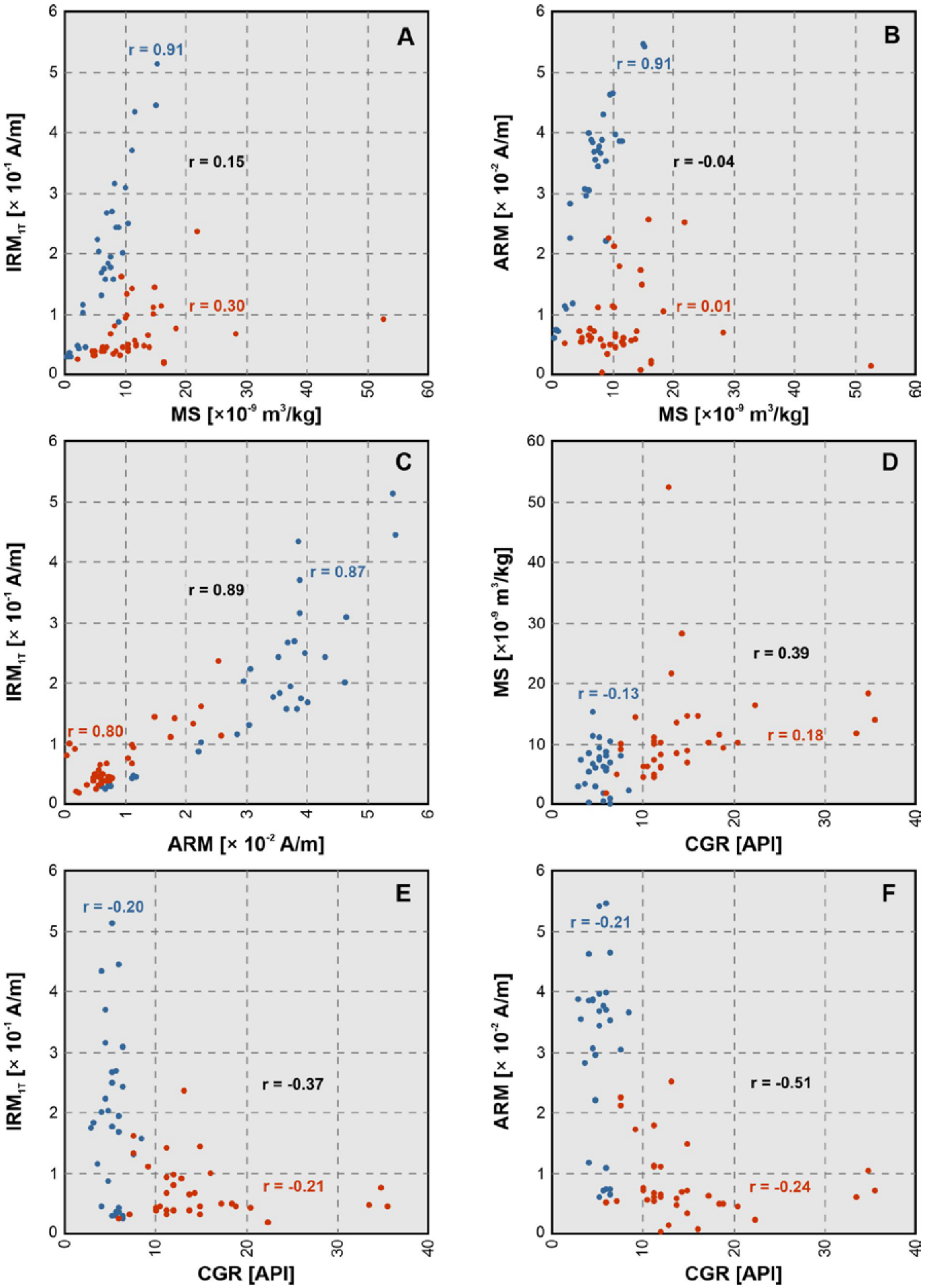

Text-fig. 4. Correlations of different rock magnetic parameters (laboratory-measured) and GRS in Lipse-tető section. A – MS vs IRM$_{1T}$; B – MS vs ARM; C – ARM vs IRM$_{1T}$; D – MS vs CGR; E – CGR vs IRM$_{1T}$; F – CGR vs. ARM. Blue dots: lower Berriasian (0–9.6 m); orange dots: upper Berriasian (9.6–21 m). ARM and IRM$_{1T}$ values are normalized to 10 g.

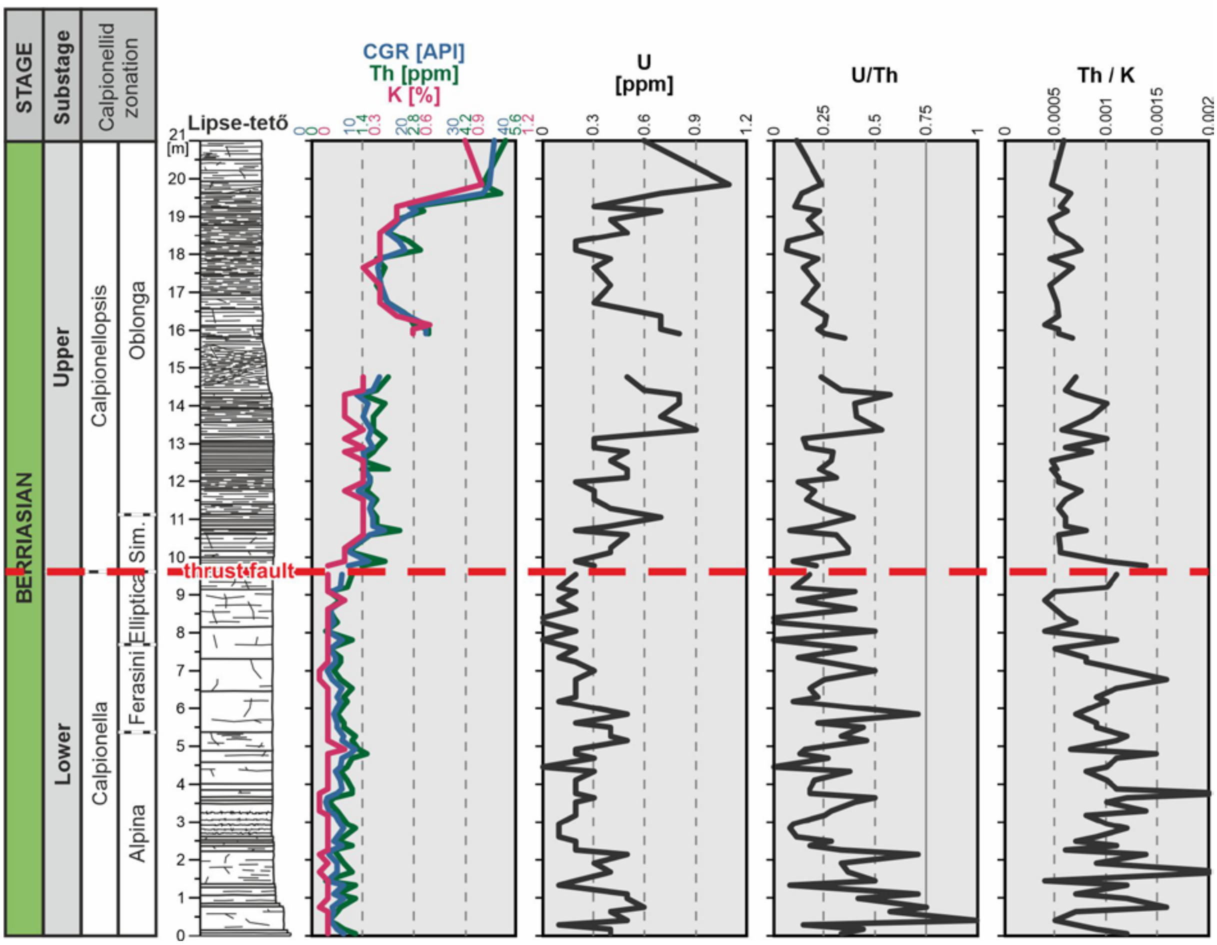

Text-fig. 5. The results of the gamma-ray spectrometry measurements in the Lipse-tető section: CGR index, Th, K and U concentrations, as well as U/Th and Th/K ratios. Abbreviations as on Text-fig. 2.

but the micritic matrix is full of microbial filaments (bacteria).

Characteristic of the calpionellid succession of the Lipse-tető section is a sudden decline in their abundance between beds 24 and 25 (right below the thrust fault), from ca. 250 specimens per thin section (in average in beds 1–24) to less than 100 specimens above. This drop is associated with a rapid decline in *C. alpina* and rather stable occurrences of other taxa (Text-fig. 2).

Although the interval above the thrust fault (9.6–20.5 m) is characterized by lower numbers of calpionellids, their assemblage is more diverse. *C. alpina* systematically occurs up to bed 36 (reaching 50% of calpionellids in bed 32), whereas *T. carpathica* maintains a stable percentage share of ca. 20% through the entire interval. Right above the thrust fault (bed 27) *Calpionellopsis simplex* occurs for the first time, already in relatively high numbers, yet it almost disappears as far as in bed 46. Ultimately, bed 32 accounts for the FO of *Calpionellopsis oblonga*; the taxon gradually gains in abundance and dominates the uppermost part of the section, above bed 43 (Text-fig. 2).

The results of the present study (on the new section of the quarry) are complementary to that of the other section (on the opposite side) which documented the lower Berriasian Calpionella elliptica and upper Berriasian Calpionellopsis oblonga subzones (Szinger and Császár 2010; Nagy and Szinger 2012).

Rock magnetism in the Lipse-tető section

The magnetic susceptibility values are rather low, mostly between 0 and 0.4×10^{-4} SI (for field measurements) and between 0 and 20×10^{-9} m^3/kg for mass normalized laboratory measurements. The lower part of the section accounts for generally lower MS values and decreasing trend (with near-zero values being reached within the 5–6.5 m interval), with characteristic local elevations around meter 2.5 (bed 11) and 6.5 (at the base of bed 22). The upper part of the section is characterized by higher MS, with well pronounced peaks right below meter 11 (cf. bed 30) and within the slump interval (14.5–16 m; beds 45–46), as well as elevated values at its top (bed 57) (Text-fig. 3).

The overall correlation between MS and laboratory-induced magnetizations (ARM and IRM_{1T}) is rather poor (Text-fig. 4A, B). However, when considering both parts of the sections separately, the poor correlation concerns mostly the upper part of the section, with higher MS and lower ARM and IRM_{1T} values. The lower part reveals a very good co-variance between MS, ARM and IRM_{1T}, therefore MS in this part of the section is carried most probably by ferromagnetic minerals. A good correlation between ARM and IRM_{1T} is observed for the entire section (Text-fig. 4C), which accounts for a fairly uniform magnetic mineralogy. Consequently, positive and usually high values of S-ratio (Text-fig. 3) indicate predomination of low coercivity minerals (magnetite).

Gamma-ray spectrometry

Lipse-tető

A consistent record of lithogenic influx to the Mecsek Basin is provided by Th and K concentrations as well as by the calculated CGR index (Text-fig. 5). The lower part of the section (0–9.6 m) accounts for a stable low terrigenous admixture (ca 0.1% K, 0.7 ppm Th and CGR index of 5 API). It increases right above the thrust fault, to ca 0.3% K, 1.4 ppm Th and CGR index of 10 API , and remains at this level up to the slump horizon. Above the slump a local peak in clastic input accounts for beds 46 and 47 (ca 16 m); it is followed by slightly lower values above and a significant increase in lithogenic input at the top of the section (above meter 19), up to ca 1% K, 5 ppm Th and CGR index of 35 API.

The lower part of the Lipse-tető section has a low (usually below 0.5 ppm) and generally decreasing contribution of U, with slightly elevated values between meters 5 and 6. It increases above the thrust fault, reaching local maximum (up to 0.9 ppm) within the slump interval (13–16 m; beds 41–47), decreases to ca 0.3 ppm in the following beds (16.5–18.5 m; beds 48–52) and increases again at the top of the section (up to 1.1 ppm in bed 56) (Text-fig. 5).

The highest U/Th values (up to 1) are characteristic of the basal 2 meters of the section. Above, the ratio decreases and remains low (ca 0.25) up to the thrust fault; only a single peak (0.7) is observed within bed 21. Corresponding low U/Th is observed also within the upper part of the section; slightly elevated values are observed only right below the slump (ca 13–14.5 m; beds 41–44). Besides, the topmost interval (above meter 16) depicts a slightly decreasing trend (Text-fig. 5).

In the case of the Th/K ratio, the lower part of the section accounts for slightly elevated values. An increasing trend is observed within the basal 3.5 meters (up to ca. 0.002), whereas generally decreasing values characterize the interval above. The Th/K values are notably lower and less variable (0.005–0.001) above the thrust fault (Text-fig. 5).

Pośrednie-Rówienka composite section

GRS measurements from the Pośrednie II, III and Rówienka sections are presented in Text-fig. 6. The new results from the Pośrednie II and Rówienka sections are summarized below, at the background of already published results from the Pośrednie III section. The lower Berriasian part (mostly section Pośrednie II) reveals a relatively low intensity of lithogenic signal, with decreasing values between the Alpina and Elliptica Subzones (M18r to uppermost M17r). The K content falls from 0.9 to 0.4%, Th – from 4 to 2 ppm, and the CGR index from 30 to 15 API. The lithogenic proxies start to rise in the Cadischiana Subzone (M17n–M16r) and then a long-term increasing trend is observed in the upper Berriasian (Rówienka section). The K, Th content and CGR index increase to 1.8%, 7.5 ppm and 60 API respectively.

The U/Th ratio reveals maximum values (0.6 to 0.7) between M17r and M16r, in the upper part of the Calpionella Zone. In the lower part of this zone moderate values from 0.4 to 0.5 are observed, while even lower values (0.3 to 0.4) occur in the upper Berriasian (Text-fig. 6).

The Th/K increases in the lower part of Pośrednie II section, reaching a maximum around the Alpina/Elliptica Subzonal boundary (lower part of M17r). Then a long term decrease is observed in the upper part of Pośrednie II and the entire Rówienka section (Text-fig. 6).

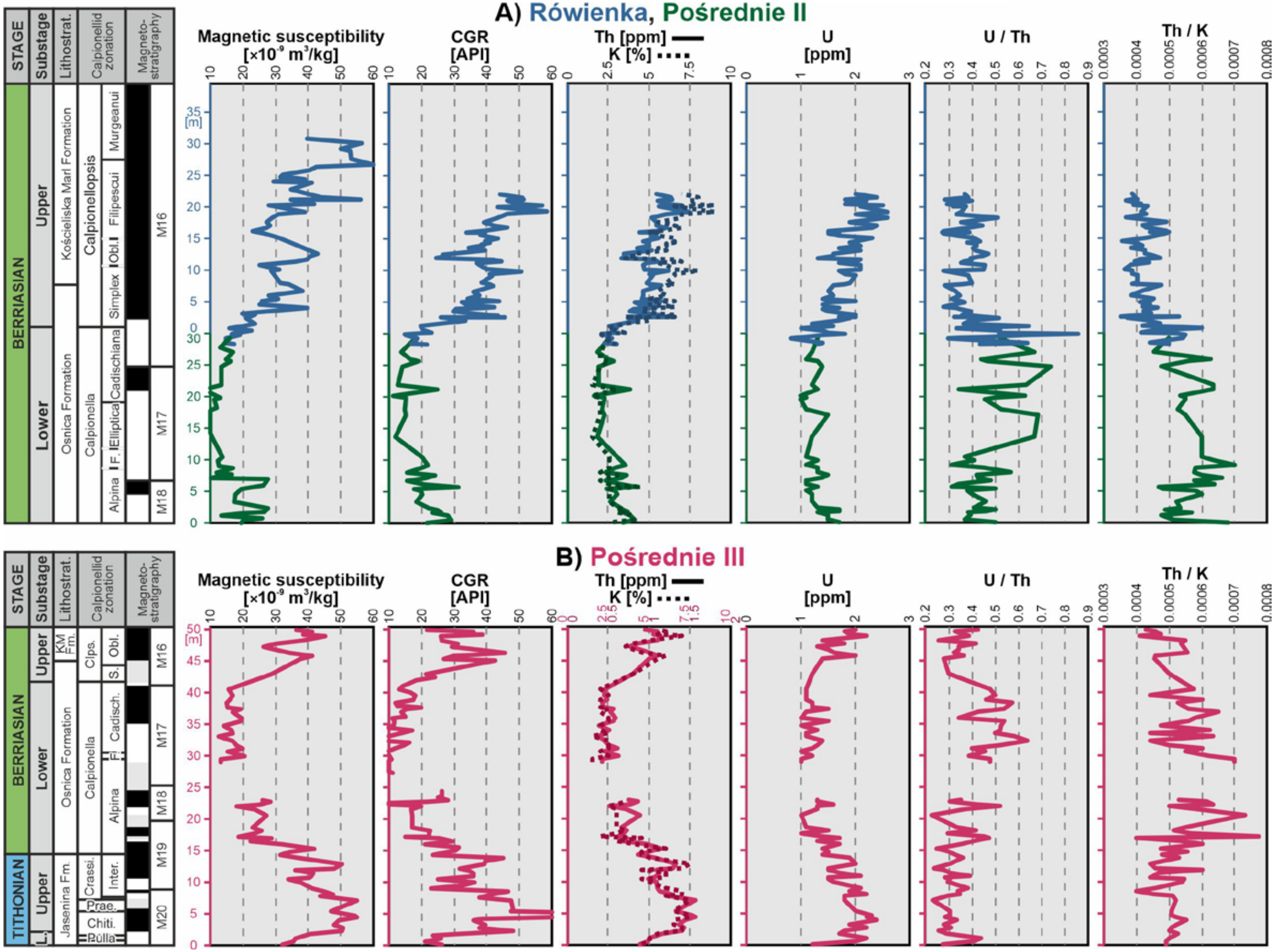

Text-fig. 6. The results of the magnetic susceptibility and gamma-ray spectrometry measurements in the sections from the Lower Sub-Tatric succession: A – Pośrednie II and Rówienka sections (new results); B – Pośrednie III section (modified after Grabowski *et al.* 2013): magnetic susceptibility, CGR index, Th, K and U concentrations, as well as U/Th and Th/K ratios.

Stable carbon and oxygen isotopes

$\delta^{13}C$ within the lower part of the Lipse-tető section reveals relatively high values (ca. 1.25‰ VPDB), with a single drop to ca 0.75‰ at bed 20 (4.9 m). The thrust fault interval (ca. 9–10 m) is characterized by notably lowered $\delta^{13}C$ values (to ca. 0.55‰). Between the thrust and slump $\delta^{13}C$ values are relatively high again, depicting a slightly decreasing trend from ca. 1.2‰ in bed 26 to 0.8‰ in base of bed 45 (slump). Above the slump, in beds 46–47, $\delta^{13}C$ decreases notably to ca. 0‰. Above, in beds 47–49, it increases again to ca. 0.9; in this context a major negative shift to -1.18‰ in bed 48 is thought to result from diagenetic alteration. Elevated values (even exceeding 1‰) remain up to bed 56, whilst the top of the studied interval (bed 57) documents another decrease to ca. 0.3‰ (Text-fig. 7).

$\delta^{18}O$ manifest strongly negative values (-2–-8‰ VPDB), which largely follow the trends documented in stable carbon isotopes (r = 0.76). The most important difference is the fact that $\delta^{13}O$ above the thrust fault is lowered for ca. 2.5‰ relative to the lower part of the section (Text-fig. 7).

INTERPRETATION AND DISCUSSION

Origin of MS signal

The raw MS signal in the Lipse-tető section does not directly follow the lithogenic trends ($r_{MS–CGR}$ = 0.39), although a lithogenic contribution to MS is quite obvious (Text-fig. 4D). The detrital MS signal is most commonly biased by authigenic ferromagnetic minerals, which might originate after pyrite (e.g., Suk *et al.* 1990). In this context, it can be noted that the generally decreasing MS, ARM and IRM_{1T} trends in the lower part of the section shows some similarities to the corresponding trend observed in U/Th (see Text-figs 3 and 5). Accordingly, the MS and magnetic mineralogy of the Lipse-tető might have been (at least to some extent) affected by authigenesis. This view is supported by the observation that the maximum share of ferromagnetic minerals (i.e., highest IRM) occurs in the lower part of the section, where lithogenic influx is the lowest (Text-fig. 4E–F and 3).

In the Pośrednie-Rówienka composite section, MS correlates well with lithogenic trends (r_{MS-CGR}:

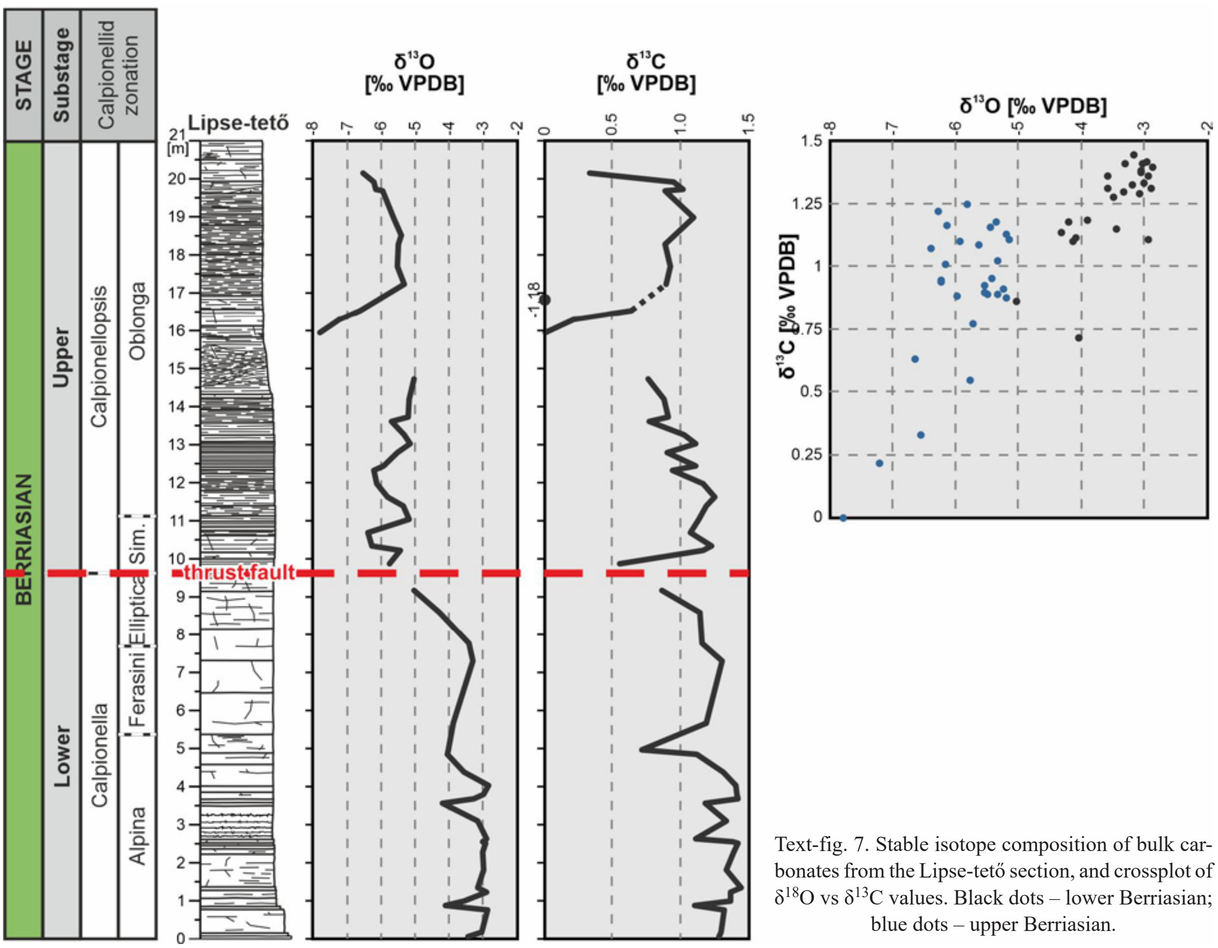

Text-fig. 7. Stable isotope composition of bulk carbonates from the Lipse-tető section, and crossplot of $\delta^{18}O$ vs $\delta^{13}C$ values. Black dots – lower Berriasian; blue dots – upper Berriasian.

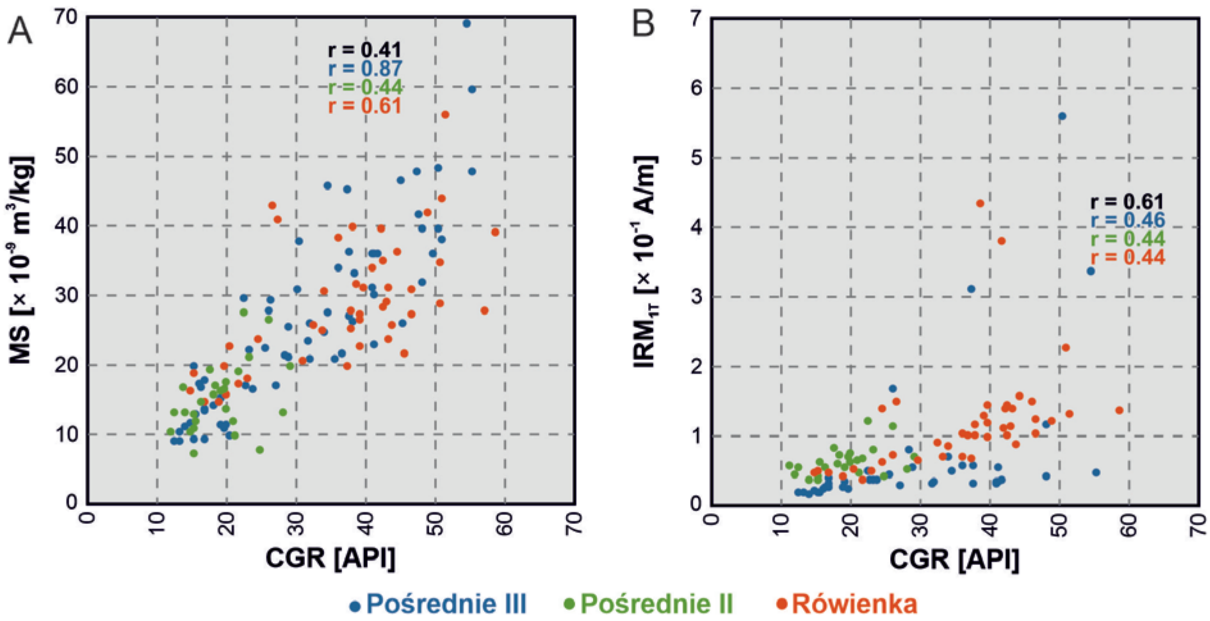

Text-fig. 8. Correlation of lithogenic influx (CGR) with (A) magnetic magnetic susceptibility (MS) and (B) isothermal remanent magnetization (IRM_{1T}) for the sections of the Lower Sub-Tatric succession. IRM_{1T} values are normalized to 10 g

0.44–0.87; Text-fig. 8A). Magnetic minerals are mostly of lithogenic origin, which may be inferred from the reasonable correlation between the CGR index and IRM_{1T} ($R_{CGR\text{-}IRM}$ ca. 0.45; Text-fig. 8B).

Chronostratigraphic calibration of GRS data from the Lower Sub-Tatric succession

Integrated bio- and magnetostratigraphic calibration enabled the plotting of selected palaeoenvironmental proxies from the Lower Sub-Tatric composite section in chronostratigraphic coordinates (Text-fig. 9). It was performed based on absolute age estimations for the Tithonian–Berriasian magnetochrons (Ogg 2020), and assuming a constant sedimentation rate throughout a single magnetochron (Grabowski and Pszczółkowski 2006). The age of each GRS measurement point was assigned according to its position against the base of the given magnetochron.

As a result, a consistent and almost continuous long-term record of CGR, MS, U/Th and Th/K was obtained (Text-fig. 9). The lithogenic input manifested by the CGR index decreases throughout the upper Tithonian, reaching minimum values around the lower/upper Berriasian boundary (see also Grabowski *et al.* 2013). A sharp increase in CGR characterizes the upper Berriasian, at least up to the upper part of the Oblonga Subzone. The MS curve mostly follows lithogenic trends. The U/Th ratio is the mirror image of the lithogenic input, with highest values around the Calpionella/Calpionellopsis zonal boundary (lower/upper Berriasian transition). Also the Th/K curve resembles that of U/Th, however, its maximum is situated slightly lower, in the middle part of the Calpionella Zone.

Stable isotope stratigraphy

As the Berriasian $\delta^{13}C$ (Text-fig. 7) values do not indicate any spectacular events (Cramer and Jarvis 2020), and the record of the Lipse-tető section is not continuous (thrust fault, slump), the isotopic results are discussed herein only briefly. Within the lower Berriasian beds, the bulk rock $\delta^{13}C$ documents a slightly decreasing trend, typical for pelagic carbonates of this age (e.g., Price *et al.* 2016; Michalík *et al.* 2021; Lodowski *et al.* 2022). Furthermore, a decreasing $\delta^{13}C$ trend observed between the Simplex and Oblonga Subzones is also known from other Tethyan successions (Grabowski *et al.* 2021b).

Strongly negative values of $\delta^{18}O$ (Text-fig. 7) account for a significant diagenetic imprint on the oxygen isotopic composition. The $\delta^{18}O$ composition is more susceptible to diagenetic alterations: therefore, its direct use as a palaeoenvironmental indicator must be performed with caution (e.g., Banner and Hanson, 1990). However, experimental data show that bulk

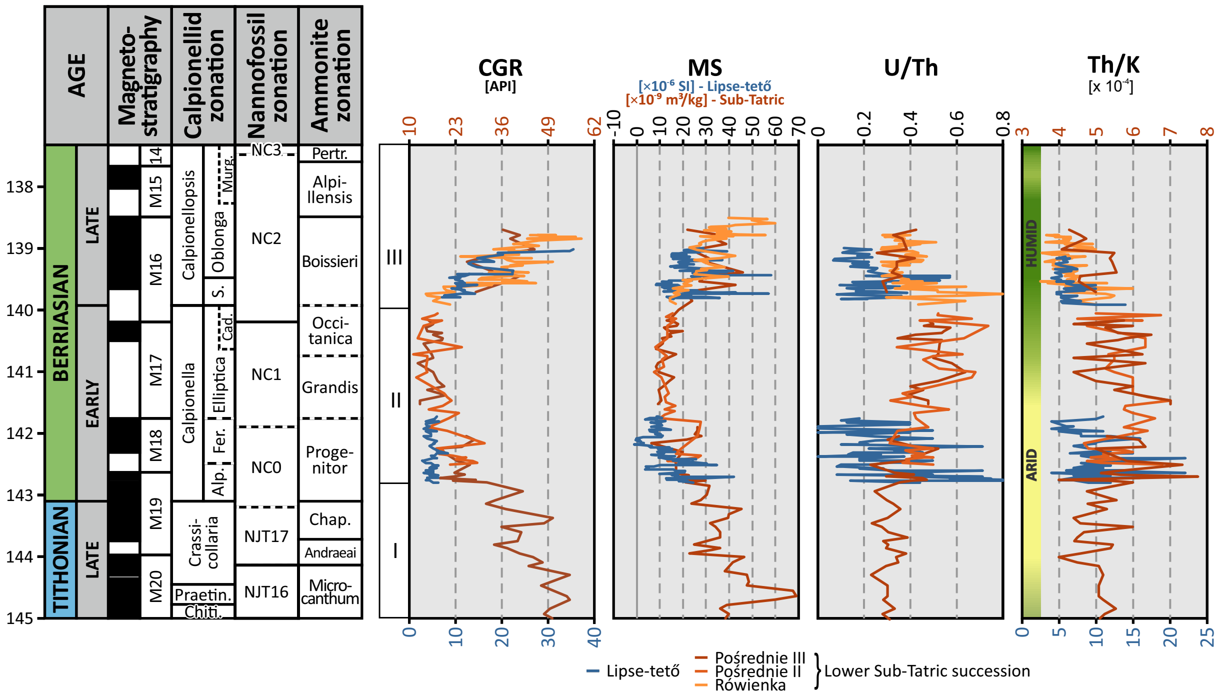

Text-fig. 9. Comparison of magnetic susceptibility, detrital influx (CGR), U/Th and Th/K ratios from the Lipse-tető section and the Lower Sub-Tatric succession (Pośrednie-Rówienka composite section) against the reference late Tithonian–Berriasian interval of the Geologic Time Scale (Ogg 2020). Palaeoenvironmental intervals I, II and III are indicated after Grabowski *et al.* (2013).

rock $\delta^{18}O$ values might faithfully reflect the relative palaeotemperature variations proved by belemnite data (e.g., Bodin *et al.* 2009; Pellenard *et al.* 2014). Concerning the lower Berriasian, mostly little variations in bulk rock $\delta^{18}O$ are observed in the Carpathian sections (Michalik *et al.* 2021) which is also the case of the Lipse-tető. The shift towards more negative values in the upper Berriasian is worth noting, however at the present state of knowledge (e.g., Grossman and Joachimski 2020) it cannot be verified, whether this represents a true palaeoenvironmental trend, a diagenetic effect or a mixture of both.

Paleoenvironmental conditions

The lower and upper Berriasian of the Lipse-tető section reveal contrasted GRS curves, rock magnetic properties, as well as microfossil frequencies. Most characteristic for the lower Berriasian are: 1) low terrigenous content (with mean of 0.1% K, 0.87 ppm Th and 4.95 API CGR); 2) elevated Th/K (with mean of 9.8×10^{-4}); 3) elevated U/Th ratio (mean = 0.31); and 4) frequent calpionellids, clearly dominated by *Calpionella alpina*. In turn, the upper Berriasian reveals: 1) high content of terrigenous elements (mean of 0.37% K, 2.20 ppm Th and 14.74 API for CGR index); 2) relatively low Th/K (mean = 6.3×10^{-4}); 3) relatively low U/Th ratio (mean = 0.25); and 4) significantly less abundant, yet more diverse calpionellids together with an upward increase of benthic forms that can be connected to the increase of detrital and nutrient input. In addition, the contrasts in clastic input (CGR index) and Th/K ratio are statistically significant, while in the case of U/Th ratio they are not as well expressed (Table 1).

Differentiation in geochemical, magnetic and biotic proxies between the lower and upper Berriasian is suggestive of changes in sedimentary environments. This view is supported by comparison with the Pośrednie-Rówienka composite section (Text-fig. 9 and Table 1; see also Grabowski *et al.* 2013). Among proxies which might inform about large-scale palaeoenvironmental perturbations, special attention is paid here to lithogenic input, Th/K ratio and calpionellid frequencies.

Lithogenic input

The changing rhythm of terrigenous supply throughout the late Tithonian–Berriasian, compati-

Section	Interval	MS [$\times 10^{-9}$ m^3/ kg]	K [%]	Th [ppm]	CGR [API]	Th/K ($\times 10^{-4}$)	U/Th
Lipse-Tető	lower Berriasian	6.16 ± 4.05	0.10 ± 0.03	0.87 ± 0.25	4.97 ± 1.18	9.80 ± 3.8	0.31 ± 0.21
	upper Berriasian	12.11 ± 8.16	0.37 ± 0.19	2.20 ± 0.93	14.74 ± 6.56	6.30 ± 1.9	0.25 ± 0.12
Pośrednie-Rówienka	lower Berriasian	16.61 ± 6.25	0.53 ± 0.17	1.27 ± 0.19	20.36 ± 5.96	5.7 ± 0.8	0.45 ± 0.11
	upper Berriasian	29.69 ± 8.73	1.11 ± 0.32	4.78 ±1.14	36.98 ± 9.47	4.40 ± 0.5	0.39 ± 0.09

Table 1. Mean magnetic susceptibility (MS) and gamma ray spectrometric results from the Lipse-tető section (Mecsek Mts) and the Pośrednie–Rówienka composite section (Lower Sub-Tatric succession). CGR – computed gamma ray index.

ble with that in the lower Sub-Tatric succession and Mecsek Mts (this study) was recently documented also in the Transdanubian Range (Grabowski *et al.* 2017; Lodowski *et al.* 2021; 2024) and in the Pieniny Klippen Belt (Grabowski *et al.* 2019). The contrast between a more carbonate lower Berriasian and a clayey upper Berriasian is the most convincingly explained by climatic trends: an arid phase during the late Tithonian–early Berriasian (e.g., Hallam *et al.* 1991; Grabowski *et al.* 2021a; Błażejowski *et al.* 2023; Lodowski and Grabowski 2023; Lodowski *et al.* 2024) and humidification at the end of the early Berriasian (e.g., Deconinck 1993; Abbink *et al.* 2001; Schnyder *et al.* 2006; Morales *et al.* 2013; Schneider *et al.* 2018). The arid climate was accompanied by stratification in the Alpine Atlantic, which is evidenced by the increased U/Th ratio (this study) and trace metal enrichments (Grabowski *et al.* 2017; Lodowski *et al.* 2024). The increase in lithogenic input during the late Berriasian was additionally enhanced by orogenic events at the northern margin of the Neotethys Ocean (uplift of the NeoTethyan Collisional Belt, e.g. Missoni and Gawlick 2011; Grabowski and Sobień 2015; Gawlick and Missoni 2019; Grabowski *et al.* 2021b). Lithogenic input in the European Platform and Arctic domains was additionally modified by "mid" Berriasian ("Ryazanian") transgression and rifting processes in northern Europe (e.g., Sladen 1983; Sladen and Batten 1984; Mutterlose *et al.* 2000; Tresch and Strasser 2010).

The occurrence of similar sedimentary trends in the Berriasian of the Mecsek Mts and the Lower Sub-Tatric succession is an additional argument for the palaegeographic affinity of both areas, likely situated on the same shelf which separated the Alpine Atlantic from the Neotethys Ocean *sensu stricto* (Text-fig. 1D). Noteworthy, lithogenic influx to the Zliechov Basin was apparently stronger than to the Mecsek Zone, as inferred from comparison of the CGR indices (Table 1). This might result from a more proximal (relative to the NeoTethyan Collision Belt) paleogeographic position of the Zliechov Basin; in this context, the Mecsek Basin was situated north of the elevated Villany Zone, which might act as a barrier for clastic material. In that case the relative palaeoposition of the Mecsek Basin might correspond rather to the zone between the North Tatric Ridge and the Pieniny Basin (Text-fig. 1). Direct comparison of lithogenic influx between the two areas is hampered by lack of magnetostratigraphic data and thus calculation of the sedimentation rate in the Lipse-tető section. The thickness of the Alpina Subzone in the Pośrednie III section amounts to 15 m, while in the Lipse-tető section the Alpina and Ferasini Subzones are 7.5 m thick (Text-fig. 2) In the Pośrednie III section, the Ferasini Subzone was not documented due to lack of the index taxon (Grabowski and Pszczółkowski 2006; Grabowski *et al.* 2013). Therefore it seems that the documented sedimentation rate in the Pośrednie III section is higher than that in Lipse-tető which conforms to the higher amount of clastic material in the former.

Calpionellid palaeoecology

It is well known that after the late Tithonian decline in crassicollarians, calpionellid assemblages become dominated by *Calpionella alpina*, which created nearly monospecific associations (e.g., Allemann *et al.* 1971; Remane *et al.* 1986; Lakova 1994; Reháková 2000). This situation changed in the latest part of Elliptica Subzone, when strong diversification of calpionellids occurred (Reháková 2000; Reháková and Michalik 1997b). Quantitative, high-resolution measurements of calpionellid abundance were perfomed by Haas *et al.* (1994) in the Sümeg section (Transdanubian Range, Hungary) for the entire Berriasian. Calpionellid frequencies apparently decrease between the lower and upper Berriasian, although the change is not linear, revealing a cyclic pattern. It was suggested that the inverse correlation between calpionellid and radiolarian frequencies, observed in Sümeg, was related to rhythmic surface productivity fluctuations controlled by orbital cycles (Haas *et al.* 1994). A corresponding explanation can be applied to the Lipse-tető section, where lithogenic influx (hence availability of nutrients) during the early and late Berriasian significantly differed.

In this context, the early Berriasian was a time of widespread oligotrophication, at least in the Western Tethyan domain (e.g., Weissert and Channell 1989; Price *et al.* 2016; Lodowski *et al.* 2024), which favored the development of calcareous micro- and nannoplankton (Tremolada *et al.* 2006). Conversely, in the late Berriasian there was a general increase in palaeoproductivity (i.e. Grabowski *et al.* 2021b), as reflected by decreasing frequencies of calpionellids and the relatively higher proportion of radiolarian (siliceous) plankton, which is generally considered to be a good indicator of high surface productivity (De Wever *et al*. 2014).

Th/K ratio as a proxy of aeolian transport?

Th/K manifests significantly contrasting values when comparing the lower and upper Berriasian intervals in both the Mecsek and the Lower Sub-Tatric successions (Table 1). The 'classical' palaeoclimatic interpretation of the Th/K ratio is that K is leached from clays (therefore Th/K increases) during more humid periods (e.g., Ruffel and Worden 2000). Such an approach has been confirmed by clay mineralogy, as elevated Th/K values correlate with increased kaolinite/illite ratios (Schnyder *et al.* 2006; Hesselbo *et al.* 2009). However, Grabowski *et al.* (2013) noted that such an interpretation contradicts the elevated Th/K in the Lower Sub-Tatric carbonates; a corresponding situation was later observed in the Transdanubian Range (Lodowski et al. 2024, Fig. 6), and now it is reported from the Mecsek Mts. This contradiction might be explained by assuming that Th constitutes an important component of the aeolian fraction (e.g., Hayes *et al.* 2013; McGee *et al.* 2016). Taking into account that an arid climate does not promote efficient riverine transport, the overall Th budget might have been dominated by wind-derived particles. Under such circumstances K-bearing minerals (i.e. feldspars) might have been easily (mechanically) destroyed, resulting in elevated Th/K (see Basu *et al.* 2009). This interpretation conforms well to the palaeoclimatic model outlined above, the "arid" early Berriasian and "humid" late Berriasian.

CONCLUSIONS

New biostratigraphic (calpionellid), rock magnetic and gamma-ray spectrometric data from the Berriasian pelagic carbonates of the Mecsek Mts (southern Hungary, Tisza Mega-unit) are presented and compared with partly published results from the Lower Sub-Tatric succession of the Tatra Mts (Poland). Magnetostratigraphic data from the Lower Sub-Tatric succession enabled chronostratigraphic calibration of magnetic susceptibility and GRS curves.

The Lipse-tetö section provides a sedimentary record of the lower (Alpina, Ferasini and lower part of Elliptica Subzones) and the upper Berriasian (upper part of the Simplex and the Oblonga Subzone). The section is cut by a thrust fault, therefore the contact between the lower and upper Berriasian is not exposed. The contrasting amount of lithogenic input (K, Th, CGR index), palaeoxygenation proxy (U/Th ratio), Th/K ratio and calpionellid frequencies and species richness between the lower and upper Berriasian, are interpreted as result of large-scale palaeoenvironmental change manifested by humidity increase, and paleotectonic phenomena (uplift of the NeoTethyan Collisional Belt) at the southern margins of the Tisza Mega-unit. The interpretation is supported by comparison with the Berriasian of the Lower-Sub-Tatric succession (Pośrednie-Rówienka composite section, Western Tatra Mts, Poland), as well as the growing amount of data from the Transdanubian Mts, Western Balkan and European Platform. The lower/upper Berriasian transition (boundary interval between the Calpionella and Calpionellopsis zones) in both areas manifested an increasing lithogenic input and a decreasing Th/K ratio. Decreased calpionellid frequencies, and their increasing species richness were documented in the upper Berriasian of the Lipse-tetö section. It is suggested that the palaeoenvironmental change caused a general increase in fertility (change from an oligotrophic to at least a mesotrophic regime), and a relative decrease of aeolian dust transport, manifested by decreasing Th/K ratio (with Th supply mostly derived from wind-blown particles).

The obtained data clearly support the idea that the same sedimentary trends might be identified in the Berriasian of the Tisza Mega-unit and of the Central West Carpathians, which accounts for their supra-regional control – interplay of tectonic events and palaeoclimatic fluctuations.

Acknowledgements

Investigations in the Lipse-tető section were financially supported by the National Science Center Poland (project no. 2016/21/B/ST/10/02941, leader: Jacek Grabowski). Investigations in the Pośrednie-Rówienka sections were performed within a frame of the Polish-French bilateral cooperation (project no. 7841/R09/R10) and a grant from Ministry of Science and

Education of Poland (project no. 683/N-POLONIUM/2010/0, leader: Jacek Grabowski). Special thanks are due to Tadeusz Sztyrak for technical assistance, as well as Istvan Főzy and Jolanta Iwańczuk for support during last phases of field work in the Mecsek Mts in 2019. The critical remarks of journal referees, Renata Jach and Ottilia Szives are gratefully acknowledged. The paper is dedicated also to Professor Géza Császár, who initiated the investigations, and passed away in December 2021.

REFERENCES

Abbink, O., Targarona, J., Brinkhuis, H. and Visscher, H. 2001. Late Jurassic to earliest Cretaceous palaeoclimatic evolution of the southern North Sea. *Global and Planetary Change*, **30**, 231–256.

Allemann, F., Catalano, R., Farès, F. and Remane, J. 1971. Standard calpionellid zonation (Upper Tithonian–Valanginian) of the western Mediterranean Province. In: Farinacci, A. (Ed.), Proceedings, II Planktonic Conference, Rome, 1970, 2, 1337–1340. Edizioni Tecnoscienza; Roma.

Banner, J.L. and Hanson, G.N. 1990. Calculation of simultaneous isotopic and trace element variations during water-rock interaction with applications to carbonate diagenesis. *Geochimica et Cosmochimica Acta*, **11**, 3123–3137.

Basu, H., Mahendra Kumar, K., Paneerselvam, S. and Chaki, A. 2009. Study of provenance characteristics and depositional history on the basis of U, Th and K abundances in the Gulcheru Formation, Cuddapah basin in Tummalapalle-Somalollapalle areas, Cuddapah-Aanantapur districts, Andhra Pradesh. *Journal of the Geological Society of India*, **74**, 318–328.

Błażejowski, B., Pszczółkowski, A., Grabowski, J., Wierzbowski, H., Deconinck, J.-F., Olempska, E., Teodorski, A. and Nawrocki, J. 2023. Integrated stratigraphy and clay mineralogy of the Owadów-Brzezinki section (Lower–Upper Tithonian transition, Central Poland): implications for correlations between the Boreal and the Tethyan domains and palaeoclimate. *Journal of the Geological Society*, **180**, DOI: 10.1144/jgs2022-073.

Bodin, S., Fiet, N., Godet, A., Matera, V., Westermann, S., Clément, A., Janssen, N.M.M., Stille, P. and Föllmi, K.B. 2009. Early Cretaceous (late Berriasian to early Aptian) palaeoceanographic change along the northwestern Tethyan margin (Vocontian Trough, southeastern France): $d^{13}C$, $d^{18}O$ and Sr-isotope belemnite and whole-rock records. *Cretaceous Research*, **30**, 1247–1262.

Casellato, C.E. and Erba, E. 2021. Reliability of calcareous nannofossil events in the Tithonian–early Berriasian time interval: implications for a revised high resolution zonation. *Cretaceous Research*, **117**, 104611.

Cramer, B.D., and Jarvis, I. 2020. Carbon isotope stratigraphy. In: Gradstein, F.M., Ogg, J.G., Schmitz, M.D. and Ogg, G.M. (Eds), Geologic Time Scale 2020, 309–344. Elsevier; Amsterdam, Oxford, Cambridge.

Császár, G. 2002. Urgon formations in Hungary with special reference to the Eastern Alps, the Western Carpathians and the Apuseni Mountains. *Geologica Hungarica Series Geologica*, **25**, 1–209.

Császár, G., Szinger, B. and Piros, O. 2013. From continental platform towards rifting of the Tisza Unit in the Late Triassic to Early Cretaceous. *Geologica Carpathica*, **64**, 279–290.

De Wever, P., O'Dogherty, L. and Gorican, S. 2014. Monsoon as a cause of radiolarite in the Tethyan realm. *Comptes Rendus Geoscience*, **346**, 287–297.

Deconinck, J.F. 1993. Clay mineralogy of the Late Tithonian–Berriasian deep-sea carbonates of the Vocontian Trough (SE France): Relationships with sequence stratigraphy. *Bulletin Centres de Recherches Exploration-Production Elf-Aquitaine*, **17**, 223–234.

Gawlick, H.-J. and Missoni, S. 2019. Sedimentary mélange formation related to ophiolitic subduction in the Alpine–Carpathian–Dinaride Mountain Range. *Gondwana Research*, **74**, 144–172.

Grabowski, J. and Pszczółkowski, A. 2006. Magneto- and biostratigraphy of the Tithonian–Berriasian pelagic sediments in the Tatra Mountains (central Western Carpathians, Poland): sedimentary and rock magnetic changes at the Jurassic/Cretaceous boundary. *Cretaceous Research*, **27**, 398–417.

Grabowski, J., Schnyder, J., Sobień, K., Koptiková, L., Krzemiński, L., Pszczółkowski, A., Hejnar, J. and Schnabl, P. 2013. Magnetic susceptibility and spectra gamma logs In the Tithonian–Berriasian pelagic carbonates In the Tatra Mts (Western Carpathians, Poland): palaeoenvironmental changes at the Jurassic/Cretaceous boundary. *Cretaceous Research*, **43**, 1–17.

Grabowski, J. and Sobień, K. 2015. Variation in clastic input in the Berriasian of the Lower Sub-Tatric (Križna) succession in the Tatra Mountains (Central Western Carpathians, Poland): data from magnetic susceptibility and inorganic geochemistry. *Annales Societatis Geologorum Poloniae*, **85**, 139–150.

Grabowski, J., Haas, J., Stoykova, K., Wierzbowski, H. and Brański, P. 2017. Environmental changes around the Jurassic/Cretaceous transition: New nannofossil, chemostratigraphic and stable isotope data from the Lókút section (Transdanubian Range, Hungary). *Sedimentary Geology*, **360**, 54–72.

Grabowski, J., Bakhmutov, V., Kdýr, Š., Krobicki, M., Pruner, P., Rehakova, D., Schnabl, P., Stoykova, K. and Wierzbowski, H. 2019. Integrated stratigraphy and palaeoenvironmental interpretation of the Upper Kimmeridgian to Lower Berriasian pelagic sequences of the Velykyi Kamianets section (Pieniny Klippen Belt, Ukraine). *Palaeogeography, Palaeoclimatology, Palaeoecology*, **532**, 1–29.

Grabowski, J., Chmielewski, A., Ploch, I., Rogov, M., Smoleń, J., Wójcik-Tabol, P., Leszczyński, K. and Maj-Szeliga, K. 2021a. Palaeoclimatic changes and inter-regional correlations in the Jurassic/Cretaceous boundary interval of the Polish Basin: portable XRF and magnetic susceptibility study. *Newsletters on Stratigraphy*, **54**, 123–158.

Grabowski, J., Stoykova, K., Wierzbowski, H. and Wójcik-Tabol, P. 2021b. Upper Berriasian chemostratigraphy, clay minerals and calcareous nannofossils of the Barlya section (Western Balkan, Bulgaria): implications for palaeoclimate and productivity changes, and stratigraphic correlations across the Alpine Tethys. *Palaeogeography, Palaeoclimatology, Palaeoecology*, **567**, 110252.

Grossman, E.L. and Joachimski, M.M. 2020. Oxygen isotope stratigraphy. In: Gradstein, F.M., Ogg, J.G., Schmitz, M.D. and Ogg, G.M. (Eds), Geologic Time Scale 2020, 279–308. Elsevier; Amsterdam, Oxford, Cambridge.

Haas, J. and Péró, C. 2004. Mesozoic evolution of the Tisza Mega-unit. *International Journal of Earth Sciences*, **93**, 297–313.

Haas, J., Kovacs, O. and Tard-Filacz, E. 1994. Orbitally forced cyclical changes in the quantity of calcareous and siliceous microfossils in the Upper Jurassic to Lower Cretaceous pelagic basin succession, Bakony Mountains, Hungary. *Sedimentology*, **41**, 643–653.

Haas, J., Kovacs, S., Gawlick, H.-J., Grădinaru, E., Karamata, S., Sudar, M., Péró, C., Mello, J., Polák, M., Ogorelec, B. and Buser, S. 2011. Jurassic evolution of the tectonostratigraphic units of the Circum-Pannonian Region. *Jahrbuch der geologischen Bundesanstalt*, **141**, 281–354.

Haas, J., Budai, T., Csontos, L., Fodor, L., Konrád, G. and Koroknai, B. 2014. Geology of the pre-Cenozoic basement of Hungary. Explanatory notes for "Pre-Cenozoic geological map of Hungary" (1 : 500 000). Geological and Geophysical Institute of Hungary; Budapest.

Hallam, A., Grose, J.A. and Ruffell, A.H. 1991. Palaeoclimatic significance of changes in clay mineralogy across the Jurassic–Cretaceous boundary in England and France. *Palaeogeography Palaeoclimatology, Palaeoecology*, **81**, 173–187.

Hardenbol, J., Thierry, J., Harley, M.B., Jacquin, Th., de Graciansky, P.-C. and Vail, P.R. 1998. Mesozoic and Cenozoic sequence Chronostraphic framework of European basins. Appendix. *SEPM Special Publication*, **60**, 763–786.

Hayes, C.T., Anderson, R.F., Fleisher, M.Q., Serno, S., Winckler, G. and Gersonde, R. 2013. Quantifying lithogenic inputs to the North Pacific Ocean using the long-lived thorium isotopes. *Earth and Planetary Science Letters*, **383**, 16–25.

Hesselbo, S.P., Deconinck, J.-F., Huggett, J.M. and Morgans-Bell, H.S. 2008. Late Jurassic palaeoclimatic change from clay mineralogy and gamma-ray spectrometry of the Kimmeridge Clay, Dorset, UK. *Journal of the Geological Society, London*, **166**, 1123–1133.

Jach, R., Djerić, N., Goričan, Š. and Reháková, D. 2014. Integrated stratigraphy of the Middle Upper Jurassic of the Križna Nappe, Tatra Mountains. *Annales Societatis Geologorum Poloniae*, **84**, 1–33.

Jach, R. and Reháková, D. 2019. Middle to Late Jurassic carbonate-biosiliceous sedimentation and palaeoenvironment in the Tethyan Fatricum domain, Križna nappe, Tatra Mts, western Carpathians. *Annales Societatis Geologorum Poloniae*, **89**, 1–46.

Jurewicz, E. 2005. Geodynamic evolution of the Tatra Mts. and the Pieniny Klippen Belt (Western Carpathians): problems and comments. *Acta Geologica Polonica*, **55**, 295–338.

Kumpan, T., Bábek, O., Kalvoda, J., Grygar, T.M. and Frýda, J. 2015. Sea-level and environmental changes around the Devonian–Carboniferous boundary in the Namur–Dinant Basin (S. Belgium, NE France): a multi-proxy stratigraphic analysis of carbonate rmap archives and its use in regional and interregional correlations. *Sedimentary Geology*, **311**, 43–59.

Lakova, I. 1994. Numerical criteria of precise delimitation of the calpionellid Crassicollaria and Calpionella Zones in relation to the Jurassic/Cretaceous system boundary. *Geologica Balcanica*, **24**, 23–30.

Lakova, I. and Petrova, S. 2013. Towards a standard Tithonian to Valanginian calpionellid zonation of the Tethyan Realm. *Acta Geologica Polonica*, **63**, 201–222.

Lefeld, J. 1974. Middle–Upper Jurassic and Lower Cretaceous biostratigraphy and sedimentology of the sub-tatric succession in the Tatra Mts (Western Carpathians). *Acta Geologica Polonica*, **24**, 277–364.

Lefeld, J., Gaździcki, A., Iwanow, A., Krajewski, K. and Wójcik, J. 1985. Jurassic and Cretaceous lithostratigraphic units of the Tatra Mountains. *Studia Geologica Polonica*, **84**, 1–93.

Lodowski, D.G., Pszczółkowski, A., Szives, O., Főzy, I. and Grabowski, J. 2022. Jurassic–Cretaceous transition in the Transdanubian Range (Hungary): integrated stratigraphy and paleomagnetic study of the Harskút and Lókút sections. *Newsletters on Stratigraphy*, **55**, 99–135.

Lodowski, D.G., Szives, O., Virág, A. and Grabowski, J. 2024. The latest Jurassic–earliest Cretaceous climate and oceanographic changes in the Western Tethys: The Transdanubian Range (Hungary) perspective. *Sedimentology*, **71**, 1843–1872.

Łuczyński, P. 2002. Depositional evolution of the Middle Jurassic carbonate sediments in the High-Tatric succession, Tatra Mountains, Western Carpathians, Poland. *Acta Geologica Polonica*, **52**, 365–378.

McGee, D., Winckler, G., Borunda, A., Serno, S., Anderson, R.F., Recasens, C., Bory, A., Gaiero, D., Jaccard, S.L., Kaplan, M., McManus, J.F., Revel, M. and Sun, Y. 2016. Tracking eolian dust with helium and thorium: impacts of grain size and provenance. *Geochimica et Cosmochimica Acta*, **175**, 47–67.

Michalík, J. 2007. Sedimentary rock record and microfacies indicators of the latest Triassic to mid-Cretaceous tensional development of the Zliechov Basin (Central western Carpathians). *Geologica Carpathica*, **58**, 443–453.

Michalík, J., Reháková, D., Halásová, E. and Lintnerová, O. 2009. A possible West Carpathian regional stratotype of the Jurassic/Cretaceous boundary (the Brodno section near Žilina). *Geologica Carpathica* **60**, 213–232.

Michalík, J., Grabowski, J., Lintnerová, O., Reháková, D., Kdyr, Š., Schnabl, P. 2021. Jurassic–Cretaceous boundary record in Carpathian sedimentary sequences. *Cretaceous Research*, **118**, 104659.

Missoni, S. and Gawlick, H.-J. 2011. Evidence for Jurassic subduction from the Northern Calcareous Alps (Berchtesgaden; Austroalpine, Germany). *International Journal of Earth Sciences*, **100**, 1605–1631.

Morales, C., Gardin, S., Schnyder, J., Spangenberg, J., Arnaud-Vanneau, A., Arnaud, H., Adatte, T. and Föllmi, K.B. 2013. Berriasian and Early Valanginian environmental chnage along a transsect from the Jura Platform to the Vocontian Basin. *Sedimentology*, **60**, 36–63.

Mutterlose, J., Brumsack, H., Flogel, S., Hay, W., Klein, C., Langrock, U., Lipinski, M., Ricken, W., Soding, E., Stein, R., Swientek, O. 2003. The Greenland–norwegian Seaway: a key area for understanding Late Jurassic to Early Cretaceous paleoenvironments. *Paleoceanography*, **18**, 1010.

Nagy, I. 1986. Investigation of Calpionellides from the Mecsek Mountains (S. Hungary). *Acta Geologica Hungarica*, **39**, 45–64.

Nagy, I. and Szinger, B. 2012. Márévár Limestone Formation. In: Főzy, I. (Ed). Lithostratigraphic units of Hungary. Jurassic, 187–189. Hungarian Geological Society; Budapest.

Nemčok, J., Bezák, V., Biely, A., Gorek, A., Gross, P., Halouzka, R., Janák, M., Kahan, Š., Kotański, Z., Lefeld, J., Mello, J., Reichwalder, P., Rączkowski, W., Roniewicz, P., Ryka, W., Wieczorek, J. and Zelman, J. 1994. Geological map of the Tatra Mountains. MŽP SR, GÚDŠ; Bratislava.

Ogg J.G. 2020. Geomagnetic Polarity Time Scale. In: Gradstein F.M., Ogg J.G., Schmitz M.D. and Ogg G.M. (Eds), Geologic Time Scale 2020, 159–192. Elsevier; Amsterdam, Oxford, Cambridge.

Pellenard, P., Tramoy, R., Pucéat, E., Huret, E., Martinez, M., Bruneau, L. and Thierry, J. 2014. Carbon cycle and sea-water palaeotemperature evolution at the Middle–Late Jurassic transition, eastern Paris Basin (France). *Marine and Petroleum Geology*, **53**, 30–43.

Petrova, S., Koleva-Rekalova, E., Ivanova, D. and Lakova I. 2019. Biostratigraphy and microfacies of the pelagic carbonate formations in the Yavorets section (Tithonian–Berriasian), Western Balkan Mts, Bulgaria. *Geologica Balcanica*, **48**, 51–73.

Petrova, S., Andreeva, P. and Lakova I. (2023). Calpionellid biostratigraphy and microfacies across the Tithonian/Berriasian boundary interval in the Western Fore-Balkan, Bulgaria. *Review of the Bulgarian Geological Society*, **84**, 193–196.

Plašienka, D. 2018. Continuity and Episodicity in the Early Alpine Tectonic Evolution of the Western Carpathians: How Large-scale Processes are Expressed by the Orogenic Architecture and Rock Recod Data. *Tectonics*, **37**, 2029–2079.

Pop, G. 1994. Calpionellid evolutive events and their use in biostratigraphy. *Romanian Journal of Stratigraphy*, **76**, 7–24.

Price, G.D., Főzy, I. and Pálfy, J. 2016. Carbon cycle through the Jurassic–Cretaceous boundary: a new global $\delta^{13}C$ stack. *Palaeogeography, Palaeoclimatology, Palaeoecology*, **451**, 46–61.

Pszczółkowski, A. 1996. Calpionellid stratigraphy of the Tithonian–Berriasian pelagic limestones in the Tatra Mts (Western Carpathians). *Studia Geologica Polonica*, **109**, 103–130.

Pszczółkowski, A. 2003. Kościeliska Marl Formation (Lower Cretaceous) in the Polish Western Tatra Mountains: lithostratigraphy and microfossil zones. *Studia Geologica Polonica*, **121**, 7–50.

Radwański A. and Szulczewski M. 1966. Jurassic stromatolites of the Villany Mountains (southern Hungary). *Annales Universitatis Scientiarum Budapestinensis de Rolando Eotvos Nominatae, Sectio Geologica*, **9**, 87–107.

Reháková, D. 2000. Calcareous dinoflagellate and calpionellid bioevents versus sea-level fluctuations recorded in the West-Carpathian (Late Jurassic/Early Cretaceous) pelagic environments. *Geologica Carpathica*, **51**, 229–243.

Reháková, D. and Michalík, J. 1997a. Evolution and distribution of calpionellids – the most characteristic constituent of lower Cretaceous Tethyan microplankton. *Cretaceous Research*, **18**, 493–504.

Reháková, D. and Michalík, J. 1997b. Calpionellid associations versus Late Jurassic and Early Cretaceous sea-level fluctuations. *Mineralia Slovaca*, **29**, 306–307.

Remane, J., Borza, K., Nagy, I., Bakalova-Ivanova, D., Knauer, J., Pop, G. and Tardi-Filacz, E. 1986. Agreement on the subdivision of the standard calpionellid zones defined at the 2nd Planktonic Conference, Roma 1970. *Acta Geologica Hungarica*, **29**, 5–14.

Rider, M.H. 1999. The Geological Interpretation of Well Logs, 288 pp. Whittles Publishing Services; Southerland, Scotland.

Ruffell, A. and Worden, R. 2000. Palaeoclimate analysis using spectral gamma-ray data from the Aptian (Cretaceous) of southern England and southern France. *Palaeogeography, Palaeoclimatology, Palaeoecology*, **155**, 265–283.

Schmid, S.M., Bernoulli, D., Fuhenschuh, D., Matenco, L., Schefer, S., Schuster, R., Tischler, M. and Ustaszewski, K. 2008. The Alpine–Carpathian–Dinaridic orogenic system: correlation and evolution of tectonic units. *Swiss Journal of Geosciences*, **101**, 139–183.

Schneider, A.C., Heimhofer, U., Heunisch, C. and Mutterlose, J. 2018. From arid to humid – the Jurassic–Cretaceous boundary interval in northern Germany. *Review of Palaeobotany and Palynology*, **255**, 57–69.

Schnyder, J., Ruffell, A., Deconinck, J.-F. and Baudin, F. 2006. Conjunctive use of spectral gamma-ray logs and clay mineralogy indefining late Jurassic–early Cretaceous palaeoclimate change (Dorset, U.K.). *Palaeogeography, Palaeoclimatology, Palaeoecology*, **229**, 303–320.

Sladen, C.P. 1983. Trends in early Cretaceous clay mineralogy in NW Europe. *Zitteliana*, **10**, 349–357.

Sladen, C.P. and Batten, D.J. 1984. Source area environments of Late Jurassic and Early Cretaceous sediments in southeast England. *Proceedings of the Geologists' Association*, **95**, 149–163.

Stampfli, G.M. and Hochard, C. 2009. Plate tectonics of the Alpine realm. In: Murphy, J.B., Keppie, J.D. and Hynes, A.J. (Eds), Ancient Orogens and Modern Analogues. *Geological Society London, Special Publications*, **327**, 89–111.

Suk, D., Peacor, D.R. and Van der Voo, R. 1990. Replacement of pyrite framboids by magnetite in limestone and implications for paleomagnetism. *Nature*, **345**, 611–613.

Szederkényi T., Haas J., Nagymarosy A. and Hámor G. 2012. Geology and History of Evolution of the Tisza Mega-Unit. In: Haas, J. (Ed.), Geology of Hungary, 103–148. Springer; Springer Berlin, Heidelberg.

Szinger, B. 2008. Early Cretaceous foraminifera from atoll environment (Márévár Valley, Mecsek Mountains, Hungary). *Hantkeniana*, **6**, 127–143.

Szinger, B. and Császár, G. 2010. Palaeontological and sedimentological investigation of the Upper Jurassic–Lower Cretaceous Márévár Limestone Formation (Eastern Mecsek). In: Dulai, A. and Bosnakoff, M. (Eds), 13th Hungarian Palaeontological Conference, Csákvár, 3–5/06/2010. Programs, abstracts, field guide, 27–28. Hungarian Geological Society; Budapest.

Szulczewski, M. 1963. Stromatolites from the High-Tatric Bathonian of the Tatra Mountains. *Acta Geologica Polonica*, **13**, 125–148.

Szulczewski, M. 1968. Stromatolity jurajskie w Polsce. *Acta Geologica Polonica*, **18**, 1–121.

Tresch, J. and Strasser, A. 2010. History of the Middle Berriasian transgression on the Jura carbonate platform: revealed by high-resolution sequence- and cyclostratigraphy (Switzerland and France). *International Journal of Earth Sciences*, **99**, 139–163.

Tremolada, F., Bornemann, A., Bralower, T.J., Koeberl, C. and van de Schootbrugge, B. 2006. Paleoceanographic changes across the Jurassic/Cretaceous boundary: the calcareous phytoplankton response. *Earth and Planetary Science Letters*, **241**, 361–371.

Vašíček, Z., Michalík, J. and Reháková, D. 1994. Early Cretaceous stratigraphy, paleogeography and life in Western Carpathians. *Beringeria*, **10**, 3–16.

Vörös, A. 2012. Episodic sedimentation on a peri-Tethyan ridge through the Middle–Late Jurassic transition (Villany Mounatins, southern Hungray). *Facies*, **58**, 415–443.

Weissert, H. and Channell, J.E.T. 1989. Tethyan carbonate carbon isotope stratigraphy across the Jurassic–Cretaceous boundary: an indicator of decelerated global carbon cycling? *Paleoceanography*, **4**, 483–494.

Manuscript submitted: 9th June 2024
Revised version accepted: 13th November 2024

PLATES 1, 2

PLATE 1

Field photos from the Lipse-tetö and Pośrednie-Rówienka sections. A – Lipse-tetö, lower Berriasian. Samples LT3 to LT17 (Alpina Subzone); B – Lipse-tetö, upper Berriasian, samples LT 37 to LT41 (Oblonga Subzone); C – Pośrednie III section, beds 74–75 (33–34 m). Cadischiana Subzone, magnetozone M17r; D – Rówienka section, bed 38 (20.5–21.5 m), Filipescui Subzone, magnetozone M16n.

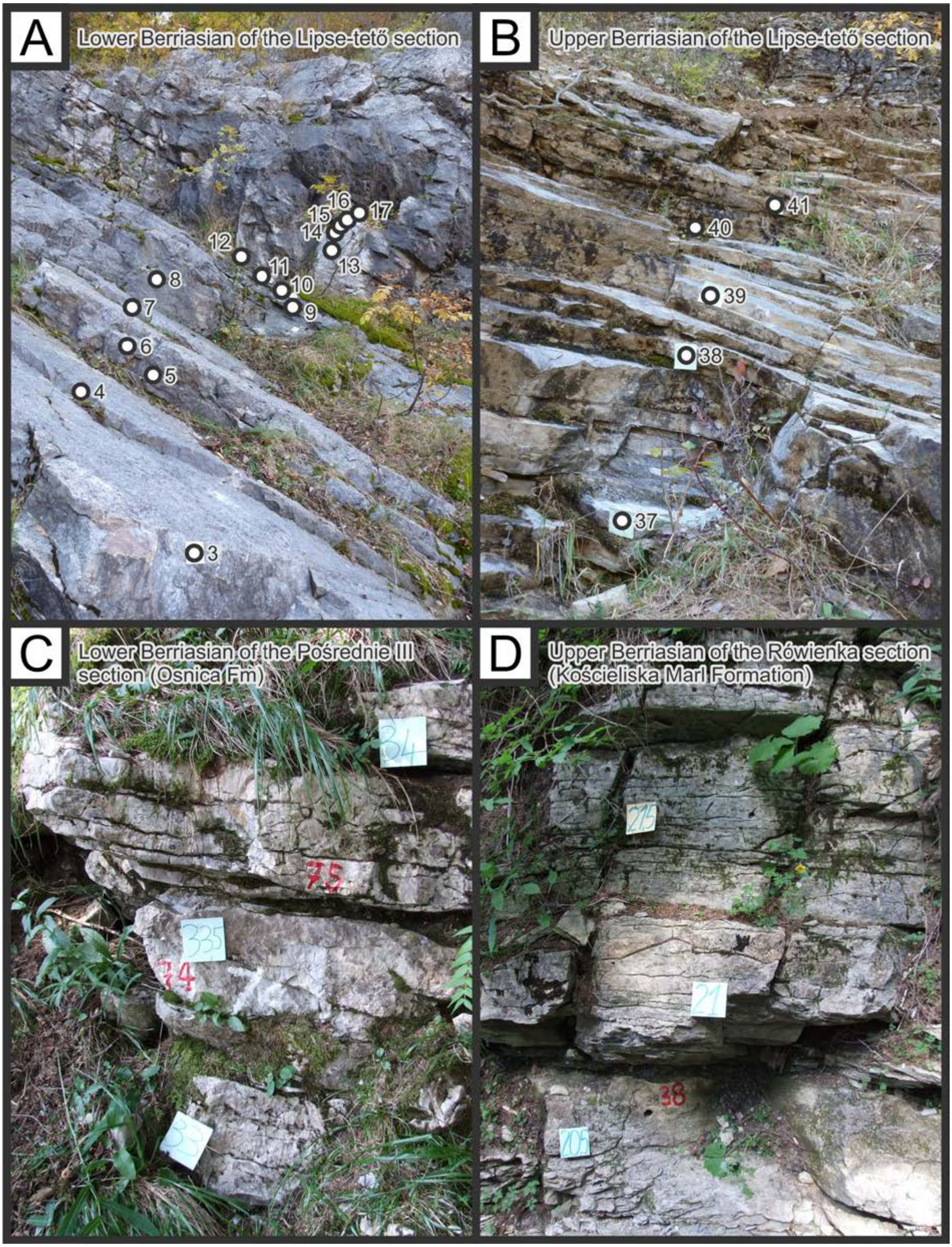
A
Lower Berriasian of the Lipse-tető section
3
4
5
6
7
8
9
10
11
12
13
14
15
16
17
B
Upper Berriasian of the Lipse-tető section
37
38
39
40
41
C
Lower Berriasian of the Pośrednie III section (Osnica Fm)
34
75
335
74
33
D
Upper Berriasian of the Rówienka section (Kościeliska Marl Formation)
275
21
38
205

PLATE 2

Calpionellids (1–10) and calcareous dinocysts of the Lipse-tető section. 1) *Crassicollaria colomi* Doben (sample LT3); 2) *Calpionella alpina* Lorenz (LT3); 3) *Tintinnopsella carpathica* Murgeanui and Filipescui (LT8); 4) *Remaniella* sp., cf. *R. catalanoi* Pop (LT21); 5) Remaniella sp., cf. *R. ferasini* (Catalano) (LT24); 6) *Remaniella* sp., *R. colomi* Pop (LT24); 7) *Calpionella elliptica* Cadisch (LT24); 8) *Calpionellopsis simplex* (Colom) (LT36); 9) *Calpionellopsis oblonga* (Cadisch) (LT32); 10) *Calpionellopsis oblonga* (Cadisch) (LT 52); 11) *Colomisphaera* ex gr. *C. carpathica–cieszynica* (LT 18); 12) *Colomisphaera carpathica* (Borza) (LT24); 13) *Colomisphaera cieszynica* (Nowak) (LT24); 14) *Cadosina* sp. (LT 36); 15) *Stomiosphaerina proxima* Řehánek (LT46).

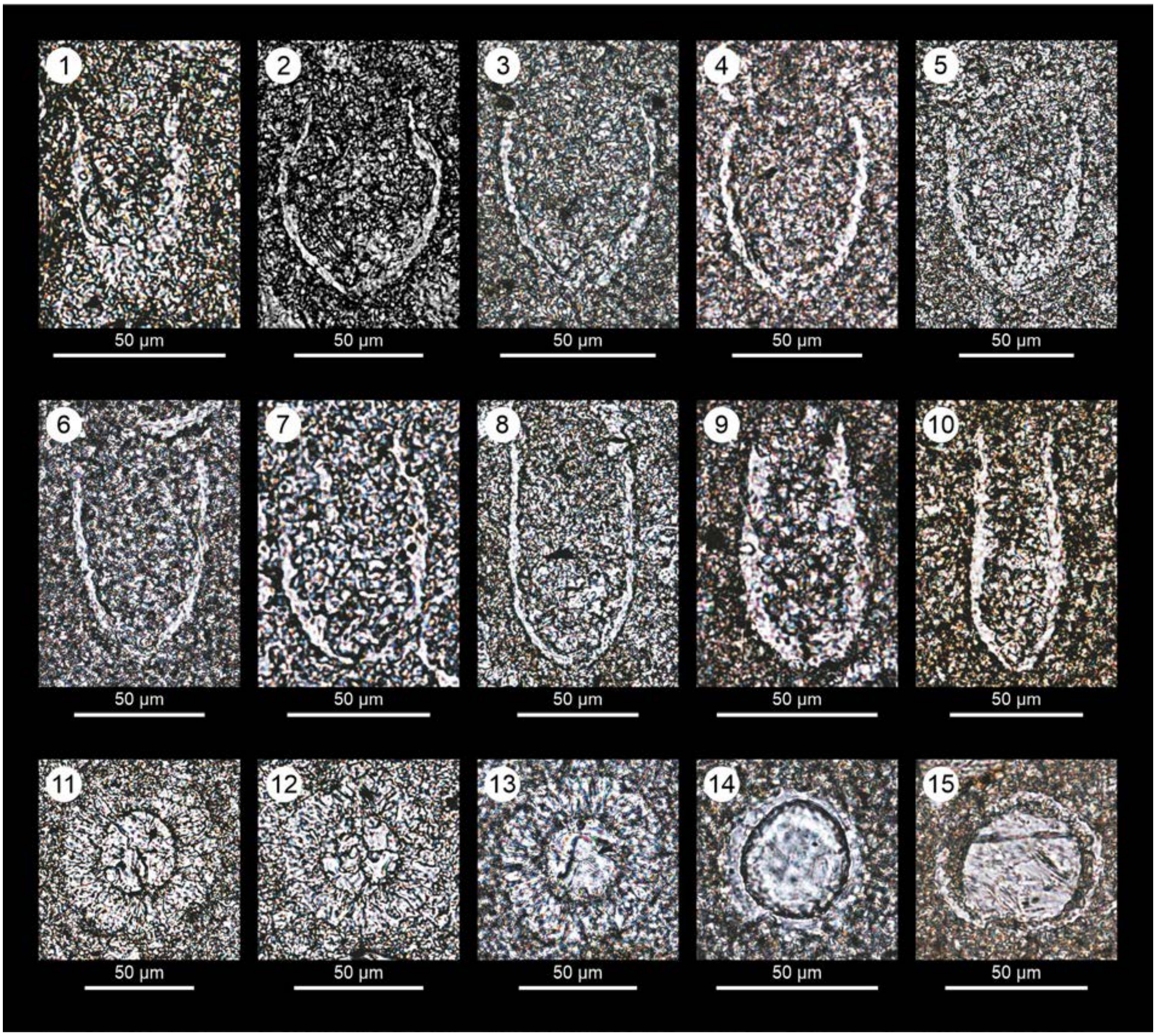
1
2
3
4
5
6
7
8
9
10
11
12
13
14
15
50 µm

Appendix 1

Lipse-tető section - GRS data												
[m]	Total		K		U		Th		Dose	CGR	U/Th	Th/K
	[ppm]	[cpm]	[%]	[cpm]	[ppm]	[cpm]	[ppm]	[cpm]	nGy/h			
0.05	93.30	360.30	0.1	36.3	0.4	9.3	1.2	10.3	7.1	6.35	0.33	0.00120
0.15	81.60	314.90	0.1	29.0	0.4	9.0	0.9	7.7	6.0	5.17	0.44	0.00090
0.25	56.30	217.30	0.1	16.7	0.1	2.8	0.7	5.9	3.1	4.38	0.14	0.00070
0.40	56.80	219.40	0.1	22.2	0.5	10.3	0.5	4.3	5.1	3.60	1.00	0.00050
0.60	67.70	261.40	0.1	19.6	0.4	7.7	0.7	6.1	4.6	4.38	0.57	0.00070
0.81	71.80	277.10	0.1	18.0	0.6	11.6	0.8	7.7	5.9	3.96	0.75	0.00160
0.95	72.10	278.40	0.1	21.4	0.5	11.4	1.2	11.1	6.8	6.35	0.42	0.00120
1.12	62.60	241.60	0.1	18.5	0.5	10.6	0.7	6.7	5.4	4.38	0.71	0.00070
1.34	72.80	281.00	0.1	24.0	0.1	4.1	1.2	10.6	5.0	6.35	0.08	0.00120
1.50	39.50	152.60	0.1	16.2	0.2	4.3	0.4	3.8	3.0	3.20	0.50	0.00040
1.70	59.10	228.00	0.1	14.4	0.4	9.0	1.1	9.8	5.4	5.14	0.36	0.00220
1.90	60.10	231.90	0.1	16.4	0.3	7.2	0.9	8.2	4.7	5.17	0.33	0.00090
2.10	62.80	242.40	0.1	10.4	0.5	10.3	0.7	6.1	4.7	3.57	0.71	0.00140
2.25	56.70	218.90	0.1	20.1	0.2	4.6	0.6	5.1	3.7	3.99	0.33	0.00060
2.42	63.50	245.30	0.1	18.5	0.2	6.7	1.1	9.5	5.0	5.96	0.18	0.00110
2.49	64.10	247.60	0.1	21.1	0.2	5.1	0.7	6.1	4.1	4.38	0.29	0.00070
2.57	60.70	234.30	0.1	23.2	0.1	3.0	0.9	7.5	4.0	5.17	0.11	0.00090
2.80	58.00	223.90	0.1	21.7	0.1	4.3	1.2	10.3	4.8	6.35	0.08	0.00120
2.97	57.90	223.60	0.1	18.0	0.1	4.8	1.0	8.8	4.4	5.56	0.10	0.00100
3.14	48.00	185.20	0.1	15.1	0.2	5.4	0.8	6.9	3.9	4.78	0.25	0.00080
3.30	42.10	162.50	0.1	13.6	0.2	5.1	0.7	6.1	3.6	3.57	0.29	0.00140
3.54	43.80	169.10	0.1	9.7	0.2	4.8	0.5	4.6	2.9	2.78	0.40	0.00100
3.63	38.50	148.70	0.1	7.0	0.3	6.1	0.6	5.6	3.3	3.17	0.50	0.00120
3.75	47.20	182.40	0.1	9.7	0.2	5.9	1.1	9.5	4.2	5.14	0.18	0.00220
3.93	69.20	267.20	0.1	25.1	0.2	5.6	1.1	9.3	5.2	5.96	0.18	0.00110
4.10	64.00	247.10	0.1	21.7	0.2	6.4	1.0	8.8	5.0	5.56	0.20	0.00100
4.30	63.50	245.30	0.1	30.8	0.3	6.4	0.8	6.7	5.2	4.78	0.38	0.00080
4.50	59.40	229.30	0.1	21.1	0.0	2.2	1.0	8.2	3.8	5.56	0.00	0.00100
4.65	73.90	285.20	0.1	33.1	0.3	7.2	1.1	9.8	6.2	5.96	0.27	0.00110
4.83	84.30	325.40	0.1	32.1	0.2	7.2	1.5	13.2	6.9	7.53	0.13	0.00150
4.95	90.60	349.60	0.2	39.9	0.2	6.9	1.3	11.1	6.9	8.37	0.15	0.00065
5.13	75.20	290.40	0.1	31.8	0.5	10.3	1.1	9.5	6.9	5.96	0.45	0.00110
5.30	80.90	312.30	0.1	37.1	0.4	9.8	1.2	10.8	7.4	6.35	0.33	0.00120
5.45	82.00	316.50	0.1	30.8	0.4	8.5	0.9	7.7	6.0	5.17	0.44	0.00090
5.61	71.20	274.70	0.1	27.7	0.2	5.1	0.9	8.2	5.0	5.17	0.22	0.00090
5.90	70.00	270.00	0.1	32.6	0.5	10.3	0.7	6.7	6.3	4.38	0.71	0.00070
6.15	59.10	228.30	0.1	15.1	0.1	3.5	1.0	8.8	3.8	5.56	0.10	0.00100
6.35	61.00	235.60	0.1	19.8	0.2	5.1	0.9	7.7	4.3	5.17	0.22	0.00090
6.56	58.30	224.90	0.1	21.4	0.2	5.4	1.1	9.5	4.9	5.96	0.18	0.00110
6.76	44.50	171.90	0.1	14.1	0.2	4.8	0.8	7.2	3.7	3.96	0.25	0.00160
6.96	54.50	210.30	0.1	14.9	0.3	6.7	0.6	5.6	3.9	3.17	0.50	0.00120
7.20	46.10	177.90	0.1	17.5	0.2	5.4	0.8	6.7	4.0	4.78	0.25	0.00080
7.41	49.90	192.80	0.1	19.6	0.1	4.1	0.8	6.7	3.8	4.78	0.13	0.00080
7.62	46.30	178.70	0.1	18.5	0.2	5.1	0.5	4.3	3.5	3.60	0.40	0.00050
7.83	47.40	182.90	0.1	24.8	0.0	1.7	1.1	9.8	4.5	5.96	0.00	0.00110
8.05	51.00	197.00	0.1	21.1	0.2	4.8	0.4	3.3	3.4	3.20	0.50	0.00040
8.24	45.60	176.10	0.1	18.3	0.0	2.2	0.7	5.9	3.1	4.38	0.00	0.00070
8.44	26.00	100.40	0.1	13.1	0.0	1.7	0.6	4.8	2.4	3.99	0.00	0.00060
8.64	53.30	205.90	0.1	26.9	0.2	5.1	0.5	4.1	4.0	3.60	0.40	0.00050
8.84	56.70	218.90	0.2	33.4	0.1	2.8	0.8	6.7	4.4	6.41	0.13	0.00040
9.04	54.30	209.80	0.1	22.7	0.2	4.3	0.5	4.1	3.5	3.60	0.40	0.00050
9.25	74.10	286.00	0.1	32.4	0.1	4.6	1.0	8.8	5.3	5.56	0.10	0.00100
9.60	75.40	291.20	0.1	30.3	0.2	6.7	1.1	9.8	5.9	5.96	0.18	0.00110
9.75	89.90	347.00	0.1	34.2	0.3	8.0	1.4	12.4	7.1	7.13	0.21	0.00140
9.90	101.40	391.40	0.2	52.7	0.2	8.0	2.0	17.1	9.3	11.12	0.10	0.00100
10.08	103.30	398.70	0.2	47.5	0.4	8.5	1.1	9.5	7.5	7.59	0.36	0.00055
10.28	107.30	414.10	0.2	47.8	0.4	9.0	1.1	9.8	7.7	7.59	0.36	0.00055
10.60	120.60	465.80	0.3	61.1	0.5	11.6	1.6	13.7	10.1	11.18	0.31	0.00053
10.70	142.00	548.20	0.3	67.3	0.2	8.2	2.4	21.0	11.2	14.33	0.08	0.00080
10.86	141.10	544.60	0.3	61.6	0.4	10.6	1.8	16.1	10.4	11.97	0.22	0.00060
11.05	143.00	552.10	0.3	71.2	0.7	15.8	1.8	16.3	12.5	11.97	0.39	0.00060
11.26	130.20	502.60	0.3	60.8	0.4	10.6	1.6	14.2	10.0	11.18	0.25	0.00053
11.50	119.50	461.30	0.3	60.5	0.3	8.5	1.8	15.5	9.7	11.97	0.17	0.00060
11.77	113.30	437.60	0.2	38.9	0.3	8.0	1.5	13.2	7.5	9.16	0.20	0.00075
11.95	112.50	434.50	0.3	63.7	0.2	6.9	1.6	14.0	9.2	11.18	0.13	0.00053
12.15	122.10	471.20	0.3	62.1	0.5	11.6	1.6	13.7	10.2	11.18	0.31	0.00053
12.28	138.60	534.90	0.3	76.7	0.5	11.6	1.4	12.4	10.9	10.40	0.36	0.00047
12.38	138.80	535.70	0.4	80.6	0.2	8.8	2.1	17.9	11.6	14.78	0.10	0.00053
12.51	123.80	477.80	0.3	64.7	0.4	10.3	1.4	12.7	9.8	10.40	0.29	0.00047
12.78	117.80	454.80	0.2	50.9	0.5	12.4	1.7	14.8	9.8	9.95	0.29	0.00085
12.95	120.70	466.00	0.3	62.9	0.3	9.5	1.8	15.8	10.2	11.97	0.17	0.00060
13.16	138.60	534.90	0.2	55.3	0.3	10.3	2.0	17.1	10.1	11.12	0.15	0.00100
13.41	165.90	640.40	0.3	77.2	0.9	20.0	1.7	15.3	13.7	11.58	0.53	0.00057
13.74	153.60	592.90	0.2	61.1	0.7	16.6	1.7	14.8	11.6	9.95	0.41	0.00085
14.07	148.80	574.30	0.2	60.5	0.8	18.2	2.0	17.4	12.5	11.12	0.40	0.00100
14.27	148.20	572.20	0.2	61.1	0.8	16.6	1.4	12.4	11.1	8.77	0.57	0.00070
14.42	152.80	590.00	0.3	76.2	0.6	14.5	1.8	16.1	12.4	11.97	0.33	0.00060
14.75	155.80	601.50	0.3	74.4	0.5	13.2	2.1	18.4	12.5	13.15	0.24	0.00070
15.09	159.00	613.80	0.3	76.2	0.8	17.1	1.4	12.7	12.4	10.40	0.57	0.00047
15.42	164.90	636.70	0.4	84.8	0.5	13.7	2.4	21.3	13.9	15.96	0.21	0.00060
15.75	177.60	685.80	0.3	77.5	0.7	16.8	2.0	17.9	13.5	12.76	0.35	0.00067
15.92	250.40	966.80	0.6	130.8	0.8	20.2	3.2	27.6	20.1	22.37	0.25	0.00053
16.00	252.40	974.60	0.6	141.2	0.7	19.7	3.2	27.8	20.8	22.37	0.22	0.00053
16.10	280.20	1081.60	0.7	145.9	0.7	18.2	2.8	24.0	19.9	22.43	0.25	0.00040
16.32	257.90	995.60	0.5	109.0	0.7	17.9	2.7	23.6	17.2	18.77	0.26	0.00054
16.72	159.60	616.10	0.4	89.5	0.3	10.6	2.1	18.4	12.8	14.78	0.14	0.00053
17.18	189.60	732.00	0.4	98.2	0.4	10.9	1.8	15.3	12.9	13.60	0.22	0.00045
17.60	149.30	576.40	0.3	72.8	0.3	8.8	2.0	17.4	11.0	12.76	0.15	0.00067
17.85	149.40	576.80	0.4	91.3	0.4	10.6	1.8	15.3	12.3	13.60	0.22	0.00045
18.13	168.10	649.10	0.4	93.0	0.2	10.6	3.0	25.7	14.6	18.32	0.07	0.00075
18.40	185.80	717.30	0.4	96.1	0.2	10.2	2.7	23.6	14.3	17.14	0.07	0.00068
18.60	188.80	728.80	0.4	98.9	0.5	13.7	2.1	18.4	14.3	14.78	0.24	0.00053
18.92	203.80	786.60	0.5	100.3	0.4	12.3	2.3	20.2	14.4	17.20	0.17	0.00046
19.15	235.00	907.30	0.5	119.5	0.7	18.6	3.1	27.1	18.8	20.34	0.23	0.00062
19.25			0.5		0.3		2.8		15.5	19.16	0.11	0.00056
19.64	347.10	1339.90	0.8	172.2	0.7	23.1	5.2	44.9	27.4	33.49	0.13	0.00065
19.80	425.60	1643.10	1.0	229.0	1.1	28.7	4.7	41.1	32.0	34.79	0.23	0.00047
21.03	392.10	1513.90	0.9	200.4	0.6	22.8	5.3	45.6	29.4	35.52	0.11	0.00059

Lipse-tető section - stable isotopes		
[m]	$\delta^{13}C$ [‰ VPDB]	$\delta^{18}O$ [‰ VPDB]
0.02	1.28	-3.47
0.11	1.29	-3.05
0.70	1.31	-2.87
0.81	1.11	-4.11
1.00	1.36	-3.57
1.12	1.36	-2.92
1.29	1.44	-3.16
1.80	1.33	-2.99
2.25	1.39	-3.03
2.42	1.42	-2.93
2.49	1.38	-3.04
2.57	1.11	-2.92
3.05	1.33	-3.17
3.54	1.18	-4.19
3.63	1.41	-3.28
3.78	1.41	-3.01
3.98	1.40	-2.84
4.30	1.31	-3.57
4.83	1.12	-4.07
4.91	0.72	-4.01
5.61	1.18	-3.88
7.24	1.30	-3.31
7.69	1.15	-3.42
8.50	1.14	-4.30
9.19	0.87	-5.02
9.82	0.55	-5.75
10.15	1.16	-5.42
10.28	1.22	-6.26
10.68	1.07	-6.37
11.00	1.13	-5.18
11.37	1.18	-5.35
11.59	1.25	-5.80
11.95	1.17	-6.11
12.32	0.94	-6.20
12.38	1.11	-5.91
12.78	0.90	-5.52
13.05	1.11	-5.13
13.23	1.02	-5.32
13.55	0.77	-5.70
13.69	0.91	-5.21
14.16	0.88	-5.18
15.32	0.76	-5.04
15.92	0.00	-7.77
16.25	0.22	-7.20
16.48	0.64	-6.61
16.72	-1.18	-7.49
17.18	0.89	-5.31
17.72	0.93	-5.52
18.25	0.89	-5.47
18.52	0.96	-5.40
18.92	1.09	-5.62
19.64	0.89	-5.95
19.70	1.02	-6.13
19.90	0.95	-6.20
20.13	0.33	-6.53

Lipse-tető section - magnetic susceptibility					
[m]	MS [x 10^{-4} SI]	[m]	MS [x 10^{-4} SI]	[m]	MS [x 10^{-4} SI]
0.00	2.46E-01	8.09	6.40E-02	17.08	2.03E-01
0.04	1.92E-01	8.19	1.00E-01	17.18	1.45E-01
0.11	1.83E-01	8.29	1.09E-01	17.28	1.85E-01
0.20	2.22E-01	8.39	1.04E-01	17.38	2.18E-01
0.30	1.87E-01	8.49	9.00E-02	17.51	2.17E-01
0.40	1.32E-01	8.59	1.02E-01	17.62	2.49E-01
0.50	1.29E-01	8.69	6.10E-02	17.73	1.86E-01
0.60	2.88E-01	8.79	9.70E-02	17.84	2.23E-01
0.70	4.20E-01	8.89	1.26E-01	17.95	1.79E-01
0.81	1.65E-01	8.99	9.70E-02	18.04	2.20E-01
0.95	1.81E-01	9.09	7.80E-02	18.14	2.46E-01
1.05	1.55E-01	9.19	3.60E-02	18.24	3.70E-01
1.12	1.49E-01	9.29	5.80E-02	18.32	2.73E-01
1.22	1.54E-01	9.39	1.10E-01	18.42	1.68E-01
1.32	9.80E-02	9.49	8.80E-02	18.52	1.57E-01
1.44	2.03E-01	9.59	9.60E-02	18.62	2.25E-01
1.53	2.08E-01			18.72	2.05E-01
1.62	2.09E-01	9.67	1.60E-01	18.82	1.50E-01
1.71	1.68E-01	9.77	1.39E-01	18.92	2.31E-01
1.80	1.59E-01	9.87	3.60E-01	19.02	1.50E-01
1.89	3.60E-02	9.97	2.92E-01	19.15	2.10E-01
1.98	5.20E-02	10.05	1.30E-01	19.27	2.14E-01
2.07	4.80E-02	10.13	1.88E-01	19.37	1.51E-01
2.16	3.90E-02	10.23	2.36E-01	19.47	1.53E-01
2.25	7.00E-02	10.33	2.00E-01	19.57	1.83E-01
2.34	7.60E-02	10.43	2.07E-01	19.67	2.10E-01
2.41	1.00E-01	10.53	1.75E-01	19.77	2.72E-01
2.49	3.48E-01	10.69	2.48E-01	19.87	2.30E-01
2.57	1.79E-01	10.76	5.70E-01	19.98	3.90E-01
2.69	3.02E-01	10.86	2.09E-01	20.08	2.42E-01
2.78	2.39E-01	10.96	4.28E-01	20.18	2.04E-01
2.87	2.48E-01	11.05	3.24E-01	20.28	2.46E-01
2.96	1.56E-01	11.17	2.60E-01	20.38	2.30E-01
3.05	1.78E-01	11.27	1.49E-01	20.48	2.88E-01
3.14	1.81E-01	11.37	1.16E-01		
3.23	2.56E-01	11.44	2.63E-01		
3.32	1.35E-01	11.54	1.51E-01		
3.41	1.06E-01	11.64	1.36E-01		
3.54	9.60E-02	11.74	1.37E-01		
3.63	1.65E-01	11.84	1.33E-01		
3.68	1.37E-01	11.94	1.54E-01		
3.78	6.20E-02	12.04	1.18E-01		
3.88	8.70E-02	12.16	1.25E-01		
3.98	1.09E-01	12.30	1.10E-01		
4.04	1.20E-01	12.39	1.43E-01		
4.14	1.07E-01	12.46	1.87E-01		
4.24	1.65E-01	12.56	1.76E-01		
4.34	9.10E-02	12.66	1.39E-01		
4.44	1.22E-01	12.76	8.50E-02		
4.54	1.20E-01	12.84	8.60E-02		
4.64	1.55E-01	12.94	1.10E-01		
4.74	9.40E-02	13.04	1.50E-01		
4.83	1.41E-01	13.11	1.49E-01		
4.91	6.00E-02	13.21	1.19E-01		
5.01	5.30E-02	13.31	1.10E-01		
5.11	6.50E-02	13.43	1.42E-01		
5.21	-2.00E-03	13.53	1.39E-01		
5.31	-9.00E-03	13.62	2.38E-01		
5.41	2.50E-02	13.74	2.34E-01		
5.51	3.20E-02	13.84	2.17E-01		
5.61	2.10E-02	13.97	2.76E-01		
5.71	1.90E-02	14.07	2.75E-01		
5.81	5.00E-03	14.17	2.77E-01		
5.91	1.40E-02	14.27	2.41E-01		
6.01	-4.00E-03				
6.11	8.00E-03	14.47	2.69E-01		
6.21	0.00E+00	14.57	2.37E-01		
6.31	2.80E-02	14.67	2.58E-01		
6.41	1.07E-01	14.77	3.10E-01		
6.54	1.08E-01	14.87	3.90E-01		
6.64	1.12E-01	14.97	5.80E-01		
6.74	1.13E-01				
6.84	8.10E-02	15.87	3.49E-01		
6.94	1.05E-01	15.97	2.41E-01		
7.04	8.00E-02	16.07	3.90E-01		
7.14	9.00E-02	16.17	2.59E-01		
7.24	5.70E-02	16.27	4.18E-01		
7.39	7.90E-02	16.37	1.86E-01		
7.49	8.90E-02	16.47	2.48E-01		
7.59	5.40E-02	16.57	2.51E-01		
7.69	1.48E-01	16.67	3.16E-01		
7.79	1.14E-01	16.77	2.97E-01		
7.89	1.14E-01	16.87	2.22E-01		
7.99	7.40E-02	16.98	1.64E-01		

Lipse-tető section - rock magnetism								
Sample	[m]	MS	NRM	ARM	IRM_{1T}	IRM_{100mT}	S-ratio	ARM/IRM_{1T}
		[x 10-9 m^3/kg]	[A/m/10g]	[A/m/10g]	[A/m/10g]	[A/m/10g]		
LT1	0.02	8.89	8.23E-04	3.52E-02	2.43E-01	-8.70E-02	0.36	0.14
LT1top	0.05	10.46	4.92E-04	3.97E-02	2.51E-01	-1.94E-01	0.77	0.16
LT2	0.11	11.05	3.63E-04	3.87E-02	3.70E-01	-1.11E-01	0.30	0.10
LT3top	0.70	11.42	7.55E-04	3.85E-02	4.34E-01	-9.47E-02	0.22	0.09
LT4	0.81	5.35	4.05E-04	3.07E-02	2.24E-01	-5.24E-02	0.23	0.14
LT6d	1.12	6.70	3.57E-04	3.83E-02	1.57E-01	-1.12E-01	0.71	0.24
LT7d	1.29	10.06	7.44E-04	4.65E-02	3.10E-01	-9.95E-02	0.32	0.15
LT7g	1.34	6.89	3.99E-04	3.68E-02	2.68E-01	-7.63E-02	0.28	0.14
LT8sr	1.80	9.46	7.19E-04	4.62E-02	2.02E-01	-1.55E-01	0.77	0.23
LT9d	2.25	8.41	6.13E-04	4.29E-02	2.44E-01	-1.36E-01	0.56	0.18
LT10d	2.38	14.92	6.07E-04	5.46E-02	4.44E-01	-2.24E-01	0.50	0.12
LT10g	2.42	8.15	2.67E-04	3.88E-02	3.16E-01	-3.90E-02	0.12	0.12
LT11	2.49	15.30	4.19E-04	5.42E-02	5.14E-01	-1.73E-01	0.34	0.11
LT12	2.57	7.85	6.33E-04	3.78E-02	2.69E-01	-1.20E-01	0.45	0.14
LT13sr	3.05	6.34	5.45E-04	3.89E-02	1.75E-01	-1.42E-01	0.81	0.22
LT14	3.54	3.02	2.30E-04	2.26E-02	1.02E-01	-8.22E-02	0.81	0.22
LT15	3.63	7.13	4.16E-04	3.55E-02	1.83E-01	-1.50E-01	0.82	0.19
LT15 dub	3.63	7.48	3.79E-04	3.44E-02	1.77E-01	-1.51E-01	0.85	0.19
LT16 3/4	3.78	7.44	4.78E-04	3.71E-02	1.95E-01	-1.30E-01	0.67	0.19
LT17g	3.98	5.60	3.09E-04	2.96E-02	2.03E-01	-8.87E-02	0.44	0.15
LT18sr	4.30	6.03	3.95E-04	4.00E-02	1.68E-01	-1.33E-01	0.79	0.24
LT19d	4.64	6.10	4.87E-04	3.04E-02	1.32E-01	-1.11E-01	0.84	0.23
LT19g	4.83	8.01	8.33E-04	3.66E-02	1.58E-01	-1.28E-01	0.81	0.23
LT20d	4.91	2.34	6.49E-05	1.10E-02	4.28E-02	-3.76E-02	0.88	0.26
LT20 3/4	5.21	-0.02	8.60E-05	6.58E-03	2.66E-02	-2.28E-02	0.86	0.25
LT20 top	5.35	0.20	1.23E-04	6.05E-03	2.99E-02	-1.99E-02	0.66	0.20
LT21 1/4	5.61	-0.11	8.02E-05	7.10E-03	3.63E-02	-1.96E-02	0.54	0.20
LT21 2/3	6.21	0.63	6.82E-05	7.34E-03	3.77E-02	-2.96E-02	0.79	0.19
LT22d	6.54	8.78	2.72E-04	2.21E-02	8.64E-02	-7.46E-02	0.86	0.26
LT22g	7.24	2.93	5.38E-04	2.84E-02	1.16E-01	-9.71E-02	0.84	0.24
LT23sr	7.69	3.41	1.88E-04	1.17E-02	4.55E-02	-3.95E-02	0.87	0.26
LT24_0.25	8.39	0.44	1.26E-04	7.48E-03	3.01E-02	-2.55E-02	0.85	0.25
LT24_0.75	8.89	0.97	1.21E-04	7.15E-03	3.01E-02	-2.39E-02	0.79	0.24
LT25 sp	9.19	1.98	1.83E-04	1.14E-02	4.76E-02	-3.42E-02	0.72	0.24
LT25 top	9.59	1.94	5.89E-05	5.11E-03	2.63E-02	-1.76E-02	0.67	0.19
LT26 sr	9.82	4.94	9.33E-05	5.52E-03	3.16E-02	-2.19E-02	0.69	0.17
LT27 top	10.15	10.14	3.94E-04	2.12E-02	1.34E-01	-9.89E-02	0.74	0.16
LT28 1/3	10.28	9.24	5.09E-04	2.25E-02	1.61E-01	-1.20E-01	0.74	0.14
LT28 top	10.60	11.06	3.11E-04	1.80E-02	1.42E-01	-1.09E-01	0.77	0.13
LT29	10.68	28.23	1.00E-04	6.98E-03	6.69E-02	-5.21E-02	0.78	0.10
LT31 bot	11.00	8.30	3.41E-04	2.75E-04	8.10E-02	-5.69E-02	0.70	0.00
LT32 top	11.37	4.59	7.33E-05	5.52E-03	3.16E-02	-2.18E-02	0.69	0.17
LT 33 sr	11.59	6.38	1.02E-04	6.16E-03	3.82E-02	-2.39E-02	0.63	0.16
LT 33 top	11.77	14.47	4.06E-04	1.73E-02	1.12E-01	-8.11E-02	0.72	0.15
LT 34 sr	11.95	7.51	1.81E-04	1.12E-02	6.79E-02	-4.55E-02	0.67	0.16
LT 35	12.15	4.93	8.54E-05	5.99E-03	3.99E-02	-2.61E-02	0.65	0.15
LT 36 g	12.32	6.33	7.89E-05	5.64E-03	4.48E-02	-2.18E-02	0.49	0.13
LT 37	12.38	6.97	1.00E-04	7.29E-03	4.61E-02	-2.96E-02	0.64	0.16
LT 38g	12.78	4.48	1.78E-04	7.28E-03	3.99E-02	-2.61E-02	0.65	0.18
LT39g	13.05	6.08	1.56E-04	6.57E-03	3.92E-02	-2.21E-02	0.56	0.17
LT40g	13.23	10.45	1.07E-04	6.82E-03	3.89E-02	-2.21E-02	0.57	0.18
LT41g	13.55	7.90	1.44E-04	5.97E-03	3.48E-02	-2.26E-02	0.65	0.17
LT42 1/3	13.69	6.32	1.07E-04	7.72E-03	4.34E-02	-2.59E-02	0.60	0.18
LT43 3/4	14.16	10.03	2.13E-04	1.14E-02	9.41E-02	-3.39E-02	0.36	0.12
LT45 10cm	14.42	10.22	2.49E-04	1.11E-02	9.72E-02	-4.25E-02	0.44	0.11
LT45 50cm	14.82	21.79	8.84E-04	2.53E-02	2.36E-01	-9.55E-02	0.41	0.11
LT45 100cm	15.32	14.57	1.79E-04	8.10E-04	9.94E-02	-3.12E-02	0.31	0.01
LT45 top	15.75	52.54	2.84E-04	1.54E-03	9.20E-02	-3.45E-02	0.38	0.02
LT46d	15.84	16.25	5.10E-05	1.92E-03	2.20E-02	-5.92E-03	0.27	0.09
LT46 10cm	15.92	16.38	2.27E-04	2.32E-03	1.81E-02	-1.22E-02	0.67	0.13
LT47 1/3	16.25	9.47	4.70E-05	4.97E-03	4.56E-02	-2.86E-02	0.63	0.11
LT47 top	16.48	11.54	1.55E-04	5.47E-03	5.73E-02	-2.88E-02	0.50	0.10
LT48	16.72	14.76	3.16E-04	1.48E-02	1.44E-01	-6.26E-02	0.43	0.10
LT49	17.18	13.67	9.37E-05	5.77E-03	6.62E-02	-1.81E-02	0.27	0.09
LT50	17.72	8.48	1.63E-04	4.73E-03	3.85E-02	-1.72E-02	0.45	0.12
LT51g	18.25	11.63	6.78E-05	4.99E-03	4.98E-02	-2.34E-02	0.47	0.10
LT52	18.52	9.03	4.07E-04	3.51E-03	3.28E-02	-1.69E-02	0.52	0.11
LT53	18.92	10.30	1.49E-04	6.26E-03	5.05E-02	-2.49E-02	0.49	0.12
LT54	19.15	10.34	6.96E-05	4.59E-03	4.28E-02	-1.13E-02	0.26	0.11
LT55	19.64	11.73	1.60E-04	6.08E-03	4.85E-02	-2.39E-02	0.49	0.13
LT56d	19.63	13.05	1.56E-04	5.71E-03	4.68E-02	-2.23E-02	0.48	0.12
LT56 top	19.90	18.32	4.66E-04	1.05E-02	7.53E-02	-4.62E-02	0.61	0.14
LT57	20.13	15.88	1.26E-03	2.57E-02	1.13E-01	-9.08E-02	0.81	0.23
LT57 top	20.45	13.99	1.26E-04	7.12E-03	4.63E-02	-2.99E-02	0.65	0.15

Lipse-tető section - quantitative calpionellid data													
Section	**[m]**	*Calpionella alpina*	*Crassicollaria parvula*	*Crassicollaria brevis*	*Tintinnopsella carpathica*	*Crassicollaria colomi*	*Calpionella* sp.	*Remaniella* sp.	*Calpionella elliptica*	*Calpionellopsis simplex*	*Calpionellopsis* sp.	*Lorenziella* sp.	*Calpionellopsis oblonga*	SUM
Lipse-tető	0.05	182	64	1	2									249
	0.6	153	84		5	1								243
	1.1	228	41		1									270
	1.8	227	29	1	1									258
	2.55	164	59		2		1							226
	3.6	197	59		10									266
	4.3	253			8		1							262
	5.1	193	18		13									224
	5.6	226	6		7			1						240
	7.2	261	28		8			1						298
	8.6	230	1		5		7	2	2					247
	9.6	20			10		2		5					37
	10	18			37				5	50	3	1		114
	10.6	17			32			2	4	10				65
	11.3	63			30			1	1	23	2		6	126
	11.6	2			15					33			7	57
	12.3	4			17			1		40	30		23	115
	12.6				6					9	1		11	27
	13.2				13			1		30	9		6	59
	14.1				24		1	1		20		1	34	81
	16.1				4						1		33	38
	17.2				17					5			49	71
	18.5				25					1			109	135
	19.6				18							1	56	75
	21				2								29	31

Lower Sub-Tatric succession - Pośrednie III																
					Total		K		U		Th		Dose			
[m]	Age [Ma]	Magneto-stratigraphy	MS [$\times10^{-9}$ m^3/kg]		[ppm]	[cpm]	[%]	[cpm]	[ppm]	[cpm]	[ppm]	[cpm]	nGy/h	CGR	U/Th	Th/K
0.00	145.525	M20r	26.12		423.2	1633.9	0.9	203.8	1.2	30.2	4.4	38.1	30	31.98	0.27	0.00049
0.50	145.450	M20r	21.06		460.6	1778.3	1.0	232.8	2.0	44.9	4.9	43.1	36.8	35.58	0.41	0.00049
0.95	145.375	M20r	25.94													
1.00	145.300	M20r			503.6	1944.3	1.0	241.8	2.2	48.6	5.0	44.6	38.7	35.97	0.44	0.00050
1.40	145.225	M20r	23.33													
1.75	145.150	M20r	31.26		482.1	1861.1	1.1	247.4	1.7	43	5.8	51	39	40.75	0.29	0.00053
2.25	145.075	?	48.42		605.7	2338.2	1.4	323.3	1.8	46.8	7.0	61.3	47.4	50.36	0.26	0.00050
2.75	145.000	M20n2n	38.01		595.4	2298.7	1.4	313.9	2.2	53.4	7.1	62.5	48.8	50.75	0.31	0.00051
3.25	144.925	M20n2n	39.73		546.9	2111.5	1.3	298	1.9	48.2	6.8	59.8	45.8	47.94	0.28	0.00052
3.75	144.850	M20n2n	36.05		577.3	2228.5	1.3	312.4	2.4	56.8	7.2	63.4	49.7	49.51	0.33	0.00055
4.00	144.775	M20n2n	38.92													
4.40	144.700	M20n2n	59.78		635.9	2454.9	1.5	334.4	2.2	54.5	7.8	68	51.6	55.13	0.28	0.00052
4.70	144.625	M20n2n	69.07		649.6	2507.7	1.5	353.8	2.3	56.4	7.6	66.9	53.2	54.35	0.30	0.00051
5.13	144.550	M20n2n	67.50													
5.38	144.475	M20n2n	47.74		617.1	2382.4	1.3	308	2.0	49.1	6.6	58.1	46.3	47.15	0.30	0.00051
5.58	144.400	M20n2n	48.42													
7.08	144.300	?	47.80		661.3	2552.9	1.5	346.1	1.8	49.1	7.8	67.8	51	55.13	0.23	0.00052
7.53	144.225	M20n1r	37.98													
7.78	144.150				512.1	1977.1	1.2	268.5	1.8	45.3	6.1	53.5	41.6	43.56	0.30	0.00051
7.97	144.075	M20n1r	41.64		574	2216	1.4	316	2.2	51.4	6.3	55	46.8	47.61	0.35	0.00045
8.47	144.000	M20n1n	46.64		541.6	2090.8	1.4	316	1.9	45.5	5.6	48.9	44	44.86	0.34	0.00040
8.97	143.950	M19r	22.88		514.1	1984.8	1.2	269.6	2.1	48.4	5.5	48.1	41.4	41.20	0.38	0.00046
9.47	143.900	M19r	32.63													
9.92	143.850	M19r	36.20		448.5	1731.3	1.0	232.4	1.6	39.6	5.4	47.5	36.4	37.54	0.30	0.00054
10.32	143.800	M19r	24.89		425.5	1642.7	0.9	211.5	1.5	36.7	4.9	42.9	33.2	33.95	0.31	0.00054
10.62	143.750				497.2	1919.4	1.2	265.4	1.5	37.1	5.3	46.2	37.8	40.41	0.28	0.00044
10.80	143.675	M19n2n	35.99		512.5	1978.3	1.2	269.2	2.1	48.4	5.4	47.5	41.2	40.81	0.39	0.00045
11.30	143.600	M19n2n	36.02		525.1	2027.2	1.2	278.8	1.7	40.9	5.6	49.2	40.3	41.59	0.30	0.00047
11.75	143.525	M19n2n	34.09		448.9	1733.2	0.9	218.4	1.5	38.6	5.4	47.3	35.1	35.91	0.28	0.00060
12.13	143.450	M19n2n	31.86		564.6	2179.6	1.4	316	1.5	40.1	6.4	55.4	44	48.00	0.23	0.00046
12.68	143.375	M19n2n	39.55		591	2281.6	1.5	331.4	2.0	48.6	6.6	57.5	47.7	50.42	0.30	0.00044
13.28	143.300	M19n2n	39.86													
13.83	143.225	M19n2n	45.37		490.7	1894.5	1.0	228.8	1.9	44.7	5.3	46.7	37.2	37.15	0.36	0.00053
14.33	143.150	M19n2n	23.54		412.6	1592.9	0.9	199.8	1.4	33.2	4.3	37.5	30.3	31.59	0.33	0.00048
14.66	143.075	M19n2n	27.65		435.9	1682.8	0.9	217.8	1.5	36.3	5.0	44.1	33.8	34.34	0.30	0.00056
15.06	143.000	M19n2n	30.41													
15.16	142.925				463.4	1788.8	1.2	268.3	1.4	36.7	5.7	50	38.7	41.99	0.25	0.00048
15.46	142.850	M19n2n	31.51													
15.99	142.800	M19n2n	20.97		390.9	1509.2	0.8	198.3	1.7	40.1	4.8	42	33	31.92	0.35	0.00060
16.49	142.770	M19n1r	29.72		313.5	1210.2	0.6	144.3	1.3	29.4	3.2	28.7	23.6	22.37	0.41	0.00053
16.89	142.750	?	25.57		367.1	1417.1	0.9	199.1	1.7	37.6	3.6	32.2	30.3	28.84	0.47	0.00040
17.02	142.730	?	14.90		266	1026.8	0.4	112.9	1.4	30.8	3.1	27.8	21.7	18.71	0.45	0.00078
17.16	142.710	M19n1n	22.38													
17.66	142.690	M19n1n	22.20		316.4	1221.6	0.6	142.9	1.0	25	3.4	30.1	22.7	23.15	0.29	0.00057
18.06	142.670	M19n1n	22.54		351.2	1355.7	0.7	175.7	1.5	34.8	3.6	32.2	28	25.57	0.42	0.00051
18.51	142.650	M19n1n	17.01		314.5	1214.1	0.6	135.5	1.1	25.8	3.3	29.3	22.3	22.76	0.33	0.00055
20.51	142.600	M18r	16.99		324.4	1252.4	0.6	140.6	1.0	28.1	4.4	38.5	25.1	27.08	0.23	0.00073
21.41	142.450	M18r	16.61		326.5	1260.5	0.6	137	1.3	30.2	3.5	31.2	23.9	23.55	0.37	0.00058
21.86	142.300	M18n	19.84													
22.01	142.250				285.7	1103	0.5	124.2	1.3	27.9	2.5	22.6	20.6	17.99	0.52	0.00050
22.21	142.200				335.5	1295.2	0.6	142.9	1.6	36.9	3.8	34.1	26.6	24.73	0.42	0.00063
22.31	142.150	M18n	6.23													
22.71	142.100	M18n	21.56		351.4	1356.6	0.7	165.3	1.3	31.3	4.3	37.7	27.5	28.32	0.30	0.00061
23.01	142.050	M18n	27.97		312.4	1205.9	0.7	157.7	1.3	31.3	3.7	32.2	25.8	25.97	0.35	0.00053
23.35	142.000	M18n	24.97													
23.65	141.950	M18n	26.20													
24.30	141.900	M18n	26.17													
27.30		?	11.02													
27.60		?	8.60													
28.10		?	7.67													
28.90	141.525	M17r	9.23		187.4	723.6	0.3	68.8	1.0	21.9	2.1	18.4	14.3	13.15	0.48	0.00070
29.35	141.450	M17r	10.56		229.2	884.8	0.3	85.1	1.0	22.7	2.1	18.4	15.6	13.15	0.48	0.00070
29.85	141.375	M17r	9.94		279.1	1077.6	0.5	112.1	1.2	27.1	3.1	27.2	20.5	20.34	0.39	0.00062
30.65	141.300	M17r	9.46		233.1	900.1	0.4	90.8	1.0	22.7	2.2	19.7	16.3	15.17	0.45	0.00055
31.05	141.225	M17r	11.52		277.2	1070.1	0.5	115.4	1.2	27.1	3.0	26.6	20.6	19.95	0.40	0.00060
31.50	141.150	M17r	14.25		258.7	998.7	0.5	113.3	1.3	28.5	2.5	22.6	20	17.99	0.52	0.00050
32.00	141.075	M17r	16.12													
32.40	141.000	M17r	9.39		245.2	946.6	0.5	111.4	1.4	28.3	2.2	20.1	19.3	16.81	0.64	0.00044
32.70	140.925	M17r	8.27													
33.00	140.850	M17r	9.28		205.8	794.4	0.3	82.6	1.1	23.9	1.9	17.4	15.6	12.36	0.58	0.00063
33.40	140.775	M17r	13.53		237.1	915.5	0.5	112.9	1.1	24.4	2.2	19.7	18.3	16.81	0.50	0.00044
34.00	140.700	M17r	16.90		219.6	847.6	0.4	96.6	1.3	27.5	2.5	22.4	18.5	16.35	0.52	0.00063
34.40	140.625	M17r	8.28													
34.70	140.550	M17r	11.22		215.5	831.8	0.4	94.1	1.0	22.3	1.9	17.2	15.9	14.00	0.53	0.00048
35.40	140.475	M17n	11.56		288.9	1115.1	0.5	119.8	1.5	32.9	2.8	24.7	22	19.16	0.54	0.00056
35.85	140.450	M17n	10.87		254.5	982.4	0.5	108.9	1.0	23.1	2.9	25.3	18.9	19.56	0.34	0.00058
36.25	140.425	M17n	14.85													
36.75	140.400	M17n	13.81		249.7	964	0.4	98.5	1.1	24.8	2.6	22.8	18	16.75	0.42	0.00065
37.25	140.375	M17n	15.34		299.4	1155.9	0.5	125.3	1.5	31.5	2.8	25.1	22.1	19.16	0.54	0.00056
37.65	140.350	M17n	19.81		233.8	902.5	0.4	107.1	1.2	25.4	2.2	19.5	18.1	15.17	0.55	0.00055
37.79	140.325	M17n	14.36													
37.81	140.300	M17n	12.54													
38.26	140.275	M17n	11.77		254	980.7	0.4	96	1.2	25.2	2.1	18.6	17.1	14.78	0.57	0.00053
38.86	140.250	M17n	17.25		247.5	955.5	0.4	102.3	1.1	24.6	2.4	21.5	18	15.96	0.46	0.00060
39.41	140.225	M17n	17.90		256.4	989.7	0.5	111.9	1.1	24.6	2.2	19.9	18.3	16.81	0.50	0.00044
39.91	140.200	M17n	16.43													
40.41	140.175	M17n	12.97		250.5	967.1	0.4	103.7	1.1	23.5	2.3	20.7	17.6	15.57	0.48	0.00058
40.99	140.150	M16r	13.94													
41.84	140.000	?	18.29													
42.34	139.850	?	23.99													
42.99	139.700	?	21.33		357.7	1380.7	0.8	178.8	1.2	30	4.0	34.7	27.5	28.78	0.30	0.00050
44.99	139.600	M16n	42.86													
45.29	139.525	M16n	27.01		472.9	1825.8	1.1	251.2	1.4	35.3	5.0	43.5	35.7	37.60	0.28	0.00045
45.79	139.450	M16n	30.06		518.9	2003.2	1.2	271.7	2.0	46.8	5.5	48.7	41.2	41.20	0.36	0.00046
46.19	139.375	M16n	45.93		447.7	1728.4	0.9	219.6	1.6	38.8	5.0	43.5	34.4	34.34	0.32	0.00056
46.79	139.300	M16n	37.95		397.6	1534.8	0.8	195.4	1.5	36.1	4.4	39.1	31.1	30.35	0.34	0.00055
47.29	139.225	M16n	29.34		325	1254.6	0.7	155.6	1.3	31.5	3.8	33.9	26.1	26.36	0.34	0.00054
47.71	139.150	M16n	31.05		390.1	1505.9	0.8	189.7	1.8	40.7	4.3	37.9	31.6	29.96	0.42	0.00054
48.29	139.075	M16n	26.36		439.5	1696.6	1.0	235.3	1.4	37.4	5.5	48.5	36.2	37.94	0.25	0.00055
48.79	139.000	M16n	25.99		557.7	2152.8	1.4	316.6	2.2	49.7	5.7	50.2	45.4	45.25	0.39	0.00041
49.09	138.925	M16n	38.73													
49.23	138.850	M16n	33.33		467.8	1806.1	1.1	249.3	1.9	43.8	5.2	45.6	38.2	38.39	0.37	0.00047
49.63	138.775	M16n	36.05		475.3	1834.8	1.2	267.7	1.8	42.8	5.5	48.5	39.9	41.20	0.33	0.00046
49.96	138.700	M16n	21.78		456.7	1763.1	1.1	253.7	2.0	45.1	4.7	41.4	38	36.42	0.43	0.00043

Lower Sub-Tatric succession - Pośrednie II																
[m]	Magneto-stratigraphy	Age [Ma]	MS [×10^{-9} m^3/kg]		Total		K		U		Th		Dose	CGR	U/Th	Th/K
					[ppm]	[cpm]	[%]	[cpm]	[ppm]	[cpm]	[ppm]	[cpm]	nGy/h			
29.14	M16r	140.050	15.700		286.2	1105	0.5	115.7	1.3	27.5	2.5	22.6	19.9	17.99	0.52	0.00050
28.14		140.070														
28.00		140.090			251.8	972.1	0.4	103.1	1.4	30	2.7	24.3	20	17.14	0.52	0.00068
27.79	M16r	140.110	12.714													
27.09	M16r	140.130	16.914		206.1	795.5	0.4	89.3	1.2	25.2	1.8	16.3	16.1	13.60	0.67	0.00045
25.87	M16r	140.160	14.796		266	1026.9	0.4	102.9	1.1	25.2	2.5	22	18.3	16.35	0.44	0.00063
25.53	M16r	140.170	16.218		291.7	1126	0.5	127.2	1.3	29.6	2.8	25.3	21.8	19.16	0.46	0.00056
25.41	M16r	140.180	15.668													
24.71	M17n	140.250	13.193		241	930.4	0.4	101.2	1.4	29.2	1.9	17.4	18.2	14.00	0.74	0.00048
21.85	M17n	140.450	13.250		199.1	768.5	0.3	83.3	1.2	25.2	1.9	17.4	15.9	12.36	0.63	0.00063
21.11		140.600	7.971		352	1358.8	0.6	144.6	1.3	30.4	3.8	33.5	25	24.73	0.34	0.00063
20.11	M17r	140.700			207.7	801.9	0.3	80.1	1.0	21	1.6	14.7	14.1	11.18	0.63	0.00053
19.83	M17r	140.750	12.936		226.9	875.8	0.4	97.5	1.1	24.2	2.2	19.9	17.2	15.17	0.50	0.00055
19.45	M17r	140.800	11.018		229	884	0.4	105	1.0	22.1	2.2	19.5	17.1	15.17	0.45	0.00055
18.23	M17r	140.900	11.834													
17.96	M17r	140.950	10.332		252.3	974.1	0.4	92.2	1.1	22.9	2.1	18.8	16.3	14.78	0.52	0.00053
17.08	M17r	141.000	7.446		255.2	985.2	0.4	104.6	1.5	30	2.2	19.5	19.1	15.17	0.68	0.00055
13.62	M17r	141.100	10.518		211.6	816.9	0.3	76.2	1.2	24.8	1.8	15.9	15	11.97	0.67	0.00060
10.42	M17r	141.350	13.711		272.8	1053.3	0.5	111.3	1.1	26	3.0	26.4	20	19.95	0.37	0.00060
9.84	M17r	141.400	11.998		265.9	1026.7	0.5	118.6	1.3	29.6	3.2	28.7	21.9	20.74	0.41	0.00064
9.12		141.450			285.2	1101.2	0.5	130.3	1.1	26.3	3.5	30.5	22.3	21.92	0.31	0.00070
8.91	M17r	141.500	12.564													
8.67	M17r	141.550	16.707		253.7	979.4	0.5	127.9	1.3	29.6	2.9	26.1	22	19.56	0.45	0.00058
7.91	M17r	141.600	11.986		247.8	956.6	0.4	108.1	1.3	28.1	2.3	20.9	19.2	15.57	0.57	0.00058
7.72	M17r	141.650	16.411													
7.54		141.675			306.8	1184.6	0.6	142.6	1.5	33.6	3.6	32.2	25.3	23.94	0.42	0.00060
7.44	M17r	141.700	12.045													
7.02	M17r	141.750	9.930		269.8	1041.5	0.5	116.3	1.4	31.1	3.3	29.3	22.2	21.13	0.42	0.00066
6.93	M18n	141.800	27.741													
6.62		141.900			253.8	979.7	0.4	105	1.1	24.6	2.3	20.1	17.9	15.57	0.48	0.00058
6.43	M18n	141.910	27.011													
6.13		141.950			277.2	1070.1	0.5	124.8	1.1	26.7	3.2	28.2	21.5	20.74	0.34	0.00064
5.88	M18n	142.050	26.163													
5.62		142.150			375.9	1451	0.9	197.4	1.3	31.3	4.2	36.8	29.5	31.19	0.31	0.00047
5.37	M18n	142.250	19.345		266.3	1028.2	0.5	114	1.2	26.9	2.4	21.6	19.4	17.59	0.50	0.00048
5.03		142.275			286	1104	0.5	126.1	1.1	24.8	2.9	25.9	20.6	19.56	0.38	0.00058
4.43	M18r	142.300	17.627		304.3	1174.9	0.5	120.7	1.2	27.7	3.0	26.6	21.1	19.95	0.40	0.00060
3.36	M18r	142.325	17.021		266.3	1028.1	0.5	111.1	1.2	26.2	2.6	23.2	19.4	18.38	0.46	0.00052
2.30	M18r	142.350	27.589		301	1161.9	0.6	138.7	1.3	30.2	3.2	28.2	23.4	22.37	0.41	0.00053
2.02		142.375			328.4	1267.6	0.7	159.2	1.7	37.5	3.4	29.9	27	24.79	0.50	0.00049
1.74	M18r	142.400	26.623		353.1	1363	0.7	171.3	1.7	37.1	3.7	32.6	28.3	25.97	0.46	0.00053
1.54	M18r	142.425	21.125		295.5	1140.6	0.6	141.8	1.3	30	3.4	29.7	23.8	23.15	0.38	0.00057
1.15	M18r	142.450	13.298		339.9	1312.2	0.8	177.6	1.5	34	3.8	33.3	28.1	27.99	0.39	0.00048
0.74	M18r	142.463	25.900													
0.40	M18r	142.475	20.039		403.3	1556.9	0.8	193.1	1.5	34.6	4.1	36.4	30	29.17	0.37	0.00051
0.00	M18r	142.500	19.213		352.1	1359.1	0.5	138.3	1.7	37.3	3.4	30.1	25.6	21.52	0.50	0.00068

Lower Sub-Tatric succession - Rówienka																
					Total		K		U		Th		Dose			
[m]	Magneto-stratigraphy	Age [Ma]	MS [×10^{-9} m^3/kg]		[ppm]	[cpm]	[%]	[cpm]	[ppm]	[cpm]	[ppm]	[cpm]	nGy/h	CGR	U/Th	Th/K
-1.70	M16n	139.900	17.27		292.6	1129.6	0.6	141.8	1.3	29.4	3.0	26.2	22.9	21.58	0.43	0.00050
-1.55	M16n	139.850	14.74		238.7	921.6	0.5	119.4	1.4	28.5	2.2	19.5	19.7	16.81	0.64	0.00044
-0.85	M16n	139.800	14.68		220.9	852.7	0.5	111.2	0.8	20.2	2.7	23.6	17.9	18.77	0.30	0.00054
-0.30	M16n	139.750	18.88		244.8	944.9	0.4	109	1.4	28.8	2.2	20.1	19.2	15.17	0.64	0.00055
-0.10	M16n	139.725	16.40		241.2	931.3	0.4	110.4	1.8	35	2.1	18.8	20.6	14.78	0.86	0.00053
0.10	M16n	139.700	18.11		296.3	1143.8	0.7	164.5	1.5	32.9	2.9	25.5	25.3	22.82	0.52	0.00041
0.50	M16n	139.675	22.66		293.5	1133.2	0.6	147.8	1.4	29.4	2.7	23.6	22.8	20.40	0.52	0.00045
0.80	M16n	139.650	15.90		241.4	931.7	0.5	127.7	1.0	23.5	3.0	26.6	20.5	19.95	0.33	0.00060
1.15	M16n	139.625	19.99		287.5	1109.7	0.6	151.4	1.6	32.3	2.5	22.2	23.5	19.62	0.64	0.00042
1.50	M16n	139.604	23.79		313.1	1208.8	0.7	167.1	1.2	27.3	3.3	29.1	24.8	24.39	0.36	0.00047
2.05	M16n	139.581			380.7	1469.8	1.0	221.3	1.7	38.2	4.3	38.3	33.3	33.22	0.40	0.00043
2.30	M16n	139.570	20.65		393.2	1518.1	1.0	236.1	1.9	41.3	3.7	32.9	34	30.86	0.51	0.00037
2.50	M16n	139.558			333.7	1288.4	0.7	177.6	1.7	37.8	3.7	33.1	29	25.97	0.46	0.00053
2.55	M16r	139.550	21.77		522.4	2016.8	1.3	302.2	2.0	48.2	6.2	54.6	44.9	45.58	0.32	0.00048
2.60	M16r	139.535			452.9	1748.5	1.2	271	1.9	42.4	4.2	37.2	37.6	36.09	0.45	0.00035
2.85	M16r	139.525	23.78		509.3	1966	1.3	288.2	2.0	47.6	5.6	48.9	42.6	43.22	0.36	0.00043
3.10	M16r	139.512	19.86		434.4	1677.2	1.1	248.1	1.8	41.5	4.9	43.5	37.1	37.21	0.37	0.00045
3.50	M16r	139.489					0.9		1.5		3.8		29.9	29.62	0.39	0.00042
3.90	M16n	139.466			381.8	1473.9	0.9	209.8	1.4	33	4.0	35.2	30.5	30.41	0.35	0.00044
4.00	M16n	139.455	39.98		439.6	1697.3	1.1	257	1.7	39.9	5.1	44.6	37.5	38.00	0.33	0.00046
4.10	M16n	139.443	35.06		475.8	1836.6	1.3	280.7	1.5	37.8	5.4	47.1	39.2	42.44	0.28	0.00042
4.50	M16n	139.420	24.98		385.8	1489.5	1.0	223.8	1.4	33.6	4.4	38.5	32.3	33.61	0.32	0.00044
4.90	M16n	139.397	25.91		405.9	1567	1.0	226.5	1.5	34.6	4.1	36.4	32.3	32.43	0.37	0.00041
5.10	M16n	139.374	25.84		499.9	1929.9	1.3	292.4	2.0	47.4	5.7	50.4	43.2	43.62	0.35	0.00044
5.50	M16n	139.351	30.67		430.2	1660.9	1.0	236.1	1.4	34.4	4.5	39.8	33.7	34.01	0.31	0.00045
6.00	M16n	139.328	27.97		453.9	1752.2	1.2	265	1.6	36.9	4.6	40	36.4	37.66	0.35	0.00038
6.60	M16n	139.305	38.39		439.7	1697.6	1.1	239.7	1.5	36.5	4.6	40.4	34.6	36.03	0.33	0.00042
7.50	M16n	139.282			488.6	1886.2	1.2	280	1.6	40.1	5.7	49.8	40.3	41.99	0.28	0.00048
7.75	M16n	139.270	34.05		471.7	1821.2	1.3	281.7	1.8	41.9	5.0	43.9	39.6	40.87	0.36	0.00038
8.00	M16n	139.259	31.64		478.1	1845.8	1.2	273.1	1.9	43	4.8	42.3	39	38.45	0.40	0.00040
9.10	M16n	139.236			491.1	1895.8	1.3	298.4	2.0	45.1	5.2	46	42.1	41.65	0.38	0.00040
9.40	M16n	139.230			487.3	1881.4	1.3	294.9	1.8	41.7	5.0	43.5	40.4	40.87	0.36	0.00038
9.80	M16n	139.220	28.77		569.1	2197	1.6	348.4	1.7	42.8	6.2	54.2	46.7	50.48	0.27	0.00039
10.15	M16n	139.213	31.14		496.4	1916.5	1.3	288	2.1	46.3	4.7	41.4	40.7	39.69	0.45	0.00036
10.80	M16n	139.190	25.21		488.5	1885.8	1.2	277.1	2.1	46.1	4.6	40.4	39.6	37.66	0.46	0.00038
11.10	M16n	139.167			423	1632.9	1.1	241.6	1.7	40.1	4.8	42.3	36	36.82	0.35	0.00044
11.35	M16n	139.155	36.34		518.8	2003	1.4	306.6	2.0	46.5	5.5	48.1	43.4	44.46	0.36	0.00039
11.60	M16n	139.144	39.77		500.8	1933.4	1.3	298.4	2.1	48.2	5.3	47.1	43.1	42.05	0.40	0.00041
11.90	M16n	139.130			323.8	1249.9	0.7	166.9	1.3	29.2	3.3	29.1	25.3	24.39	0.39	0.00047
12.15	M16n	139.125	40.86		351.6	1357.5	0.8	183.7	1.6	35.3	3.6	31.8	28.5	27.20	0.44	0.00045
12.50	M16n	139.121	42.96		347.7	1342.2	0.8	178.2	1.6	35.3	3.4	30.1	27.8	26.42	0.47	0.00043
13.15	M16n	139.110			505.5	1951.6	1.2	283	2.1	48.2	5.1	45	41.6	39.63	0.41	0.00043
13.55	M16n	139.105			435.9	1682.8	1.1	251	1.7	39	4.2	36.6	35.2	34.46	0.40	0.00038
13.90	M16n	139.098			478.5	1847.1	1.2	269.2	2.1	47.2	5.0	43.9	40.1	39.23	0.42	0.00042
14.10	M16n	139.093			496.4	1916.3	1.2	274.6	2.0	45.5	4.8	42.7	39.8	38.45	0.42	0.00040
14.35	M16n	139.088			484.6	1870.9	1.3	297.8	1.9	42.8	5.0	43.5	40.9	40.87	0.38	0.00038
14.60	M16n	139.075			478	1845.4	1.3	285.7	2.0	45.3	4.6	40.8	40.1	39.29	0.43	0.00035
15.05	M16n	139.052	31.29		521.4	2013	1.3	302.6	2.3	52.2	5.6	49.2	44.8	43.22	0.41	0.00043
15.50	M16n	139.029			455.8	1759.7	1.1	252.7	1.7	41.1	5.1	44.8	37.6	38.00	0.33	0.00046
15.70	M16n	139.020	26.47		443.2	1711	1.1	255	1.5	38.4	5.4	47.5	37.6	39.17	0.28	0.00049
15.90	M16n	139.006			455.5	1758.5	1.1	258.5	1.5	37.8	5.5	47.9	37.8	39.57	0.27	0.00050
16.00	M16n	139.000			418.8	1616.8	1.0	231.1	1.7	38.6	4.4	39.1	34.3	33.61	0.39	0.00044
16.15	M16n	138.983	22.85		445.2	1718.6	1.1	248.5	1.5	38.6	5.4	47.5	37.2	39.17	0.28	0.00049
16.70	M16n	138.960	27.24		553.1	2135.3	1.4	320.6	2.3	52.2	6.0	52.7	46.8	46.43	0.38	0.00043
17.00	M16n	138.937	28.26		515	1988.2	1.3	293.2	2.4	53.4	5.4	48.1	44.3	42.44	0.44	0.00042
17.50	M16n	138.914	27.23		463.6	1789.6	1.1	255	1.9	44.2	5.4	47.7	39.2	39.17	0.35	0.00049
18.20	M16n	138.891	29.17		556.7	2149.3	1.4	318.5	2.6	55.7	5.1	45	46	42.89	0.51	0.00036
18.90	M16n	138.868	30.89		549.8	2122.3	1.4	312.8	2.0	48	6.0	52.5	45.2	46.43	0.33	0.00043
19.25	M16n	138.845	39.04		660	2548.1	1.8	410.3	2.6	60.6	7.4	65	57.8	58.46	0.35	0.00041
20.00	M16n	138.822			545.9	2107.3	1.3	306.2	2.1	48.2	5.6	49.6	44.2	43.22	0.38	0.00043
20.15	M16n	138.810			590.6	2280.1	1.6	367.4	2.2	53.9	6.9	60.7	52.2	53.23	0.32	0.00043
20.30	M16n	138.805	27.82		644.8	2489.5	1.8	397.1	2.5	57.6	7.0	61.3	55.4	56.89	0.36	0.00039
20.50	M16n	138.799	41.96		568.2	2193.6	1.5	337.1	1.8	44.2	6.2	54	46.2	48.85	0.29	0.00041
21.00	M16n	138.790			567.1	2189.2	1.5	343.4	2.2	49.3	5.5	48.3	46.7	46.10	0.40	0.00037
21.07	M16n	138.788	34.83		607.9	2346.6	1.6	365.9	2.2	50.7	6.2	54.6	50	50.48	0.35	0.00039
21.15	M16n	138.785	56.18		578.1	2231.9	1.6	359.2	1.8	45.1	6.4	55.8	48.4	51.26	0.28	0.00040
21.50	M16n	138.775	44.04		621.2	2398.1	1.6	369.1	2.4	55.5	6.3	55.4	51.6	50.87	0.38	0.00039
22.00	M16n	138.765			538.9	2080.3	1.4	312.2	2.0	46.5	5.4	47.5	43.7	44.07	0.37	0.00039